Replacement of a Naphthalene Scaffold in Kelch-like ECH-Associated Protein 1 (KEAP1)/ Nuclear factor (erythroid-derived 2)-like 2 (NRF2) Inhibitors

Benjamin G. Richardson[†], **Atul D. Jain**[†,ǁ], **Haranatha Potteti**[‡], **Phillip R. Lazzara**[†], **Brian P. David**[†], **Chandra Tamatam**[‡], **Ewelina Choma**[†], **Kornelia Skowron**[†], **Katherine Dye**[§], **Zamia Siddiqui**[†], **Yue-Ting Wang**[§], **Aleksej Krunic**[†], **Sekhar P. Reddy**[‡,#], and **Terry W. Moore**[†,§,#,*]

[†]Department of Medicinal Chemistry and Pharmacognosy, College of Pharmacy, University of Illinois at Chicago, 833 S. Wood Street, Chicago, IL, 60612;

[‡]Department of Pediatrics, College of Medicine;

[§]UICentre for Drug Discovery;

[#]University of Illinois Cancer Center; University of Illinois at Chicago, 833 S. Wood Street, Chicago, IL, 60612

Abstract

Activators of Nuclear factor-erythroid 2-related factor 2 (NRF2) could lead to promising therapeutics for prevention and treatment of oxidative stress and inflammatory disorders. Ubiquitination and subsequent degradation of the transcription factor NRF2 is mediated by Kelch-like ECH-associated protein-1 (KEAP1). Inhibition of the KEAP1/NRF2 interaction with small molecules leads to NRF2 activation. Previously, we and others described naphthalene-based NRF2 activators, but the 1,4-diaminonaphthalene scaffold may not represent a drug-like scaffold. Paying particular attention to aqueous solubility, metabolic stability, potency, and mutagenicity, we modified a previously known, naphthalene-based non-electrophilic NRF2 activator to give a series of non-naphthalene and heterocyclic scaffolds. We found that, compared to previously reported naphthalene-based compounds, a 1,4-isoquinoline scaffold provides a better mutagenic profile without sacrificing potency, stability, or solubility.

Table of contents Graphic

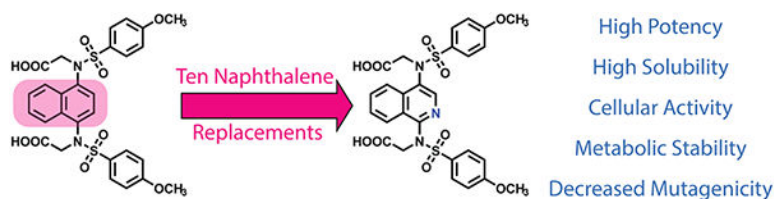[*]**Corresponding Author:** twmoore@uic.edu. Phone: (312) 413-1846. Fax: (312) 996-7107;.
[ǁ]current address: Center for Molecular Innovation and Drug Discovery, Northwestern University, Evanston, IL 60208

Introduction:

Detoxification enzymes act as the cell's main defense mechanism to counter oxidative and electrophilic stress. Detoxification enzymes include, but are not limited to, NAD(P)H quinone oxidoreductase 1 (NQO1), heme oxygenase 1 (HMOX1), glutamate-cysteine ligase-modifier and—catalytic subunits (GCLM and GCLC), and glutathione *S*-transferases (GST). The transcription of these and other genes is regulated by the transcription factor, NRF2 (nuclear factor-erythroid2-related factor 2), a member of the cap 'n' collar family of basic leucine zipper proteins. Endogenous NRF2 levels are maintained by KEAP1 (Kelch like ECH associated protein 1), which acts as a negative regulator of NRF2. KEAP1 is a 69 kDa protein that exists as a homodimer, and it contains 27 cysteine residues, which act as sensors for oxidative or electrophilic stressors.[1, 2, 3] In the absence of oxidative or electrophilic stressors, NRF2 is degraded by the E3 ubiquitin ligase Cullin 3 (CUL3), which binds to KEAP1's BTB domain (Figure 1A).[4] KEAP1 functions as a substrate adaptor protein, by bridging NRF2 to CUL3. A lysine-rich region located between ETGE and DLG motifs of NRF2 is well-positioned for ubiquitination, and NRF2 is subsequently degraded through the ubiquitin/proteasome system.[5–9] Inhibition of the KEAP1/NRF2 interaction prevents this ubiquitination and degradation, leading to an increase in NRF2 levels. NRF2 then translocates to the nucleus, heterodimerizes with the small MAF (sMAF) transcription factors and binds to antioxidant response elements (AREs) in the promotor regions of many detoxification genes;[2, 5, 10–15] thus, inhibitors of the KEAP1/NRF2 interaction serve as NRF2 activators.

Oxidative and electrophilic stressors induce transcription of detoxification enzymes by disrupting the interaction of NRF2 and KEAP1, but they do so indirectly. Three prevailing mechanisms exist to explain this disruption, namely: 1) the CUL3 dissociation model, 2) the hinge and latch model, and 3) the conformational cycling model.[6, 8, 9, 16, 17] In all three models, a KEAP1 homodimer binds to a single NRF2 molecule through high affinity ETGE and low affinity DLG motifs within the Neh2 domain of NRF2. Under electrophilic stress, modification of specific cysteine sulfhydryl groups leads to loss of CUL3, displacement of NRF2's DLG motif, or a non-optimal conformation for ubiquitination. In the CUL3 dissociation model, a cysteine in the BTB domain, Cys151, of KEAP1 is modified, leading to dissociation of CUL3 from KEAP1, preventing NRF2 ubiquitination (Figure 1B). The hinge and latch model is triggered through electrophilic modification of cysteine residues in Keap1's IVR region, rather than the BTB domain of KEAP1. This modification changes KEAP1's conformation causing release of the DLG motif, while NRF2 remains bound at the ETGE motif "hinge." According to this model, release of the DLG motif "latch" results in a binding pose of NRF2 that is inaccessible for ubiquitination (Figure 1C). In the conformational cycling model, all of the partners are still bound to one another, but covalent

modification of KEAP1 brings about conformational changes in KEAP1 and NRF2 that disfavor ubiquitination of NRF2 (Figure 1D).[17] All of these models result in an inability to ubiquitinate and degrade NRF2 in the cytosol, leading to NRF2 translocation into the nucleus. NRF2 then complexes with small MAF proteins, binds to antioxidant response elements, and transcribes the above mentioned detoxification enzymes.[2, 10, 11, 14]

Due to the role of NRF2 in cytoprotection, several NRF2 activators have been tested in the clinic against a number of disease states.[18–20] All of these clinical candidates have utilized the same mechanism of action: an electrophile is introduced to interact with the sulfhydryl groups of KEAP1 and activate NRF2. Several NRF2 activators have proceeded as far as phase III clinical trials with a few making it into clinical use; however, many of these electrophilic compounds may have selectivity issues. For instance, both sulforaphane (**3**) and a bardoxolone (**1**) may have hundreds of molecular targets (Chart 1).[21, 22] Similarly, Schulze-Topphoff et al. have shown that the mechanism of action of dimethyl fumarate **2** (Tecfidera®, Chart 1) in multiple sclerosis may be independent of the KEAP1/NRF2 axis.[23] A selective, non-electrophilic molecule could be useful to disentangle the contribution of NRF2 activation against a particular pathophysiological state.[24]

The binding sites of NRF2's ETGE and DLG motifs on KEAP1 represent "hot spots" that can be targeted with non-electrophilic small molecules and peptides. This route differs from the electrophilic mechanism of NRF2 activation, and may provide advantages in terms of on-target selectivity.[19, 25–27] We and others have previously reported several NRF2 activators that use a 1,4-substituted naphthalene core.[1, 16, 28–30] These compounds show low nanomolar potencies *in vitro* and increase transcription of NRF2 target genes in cells; however, the 1,4-diaminonaphthalene core imparts properties that may negatively impact the development of these molecules. For instance, Winkel et al. showed that naphthalene **4** (RA-839) was active in vivo only if Phase 1 metabolism were inhibited (Chart 2).[31] Naphthalene itself is metabolically activated to naphthalene oxide and naphthoquinones, and others have shown that it can covalently react with proteins *in vitro* and *in vivo*.[32–35] Additionally, some aminonaphthalenes show carcinogenic and mutagenic properties.[36, 37] Taken together, these findings suggest that the central naphthalene scaffold may not be an optimal core for this series of compounds.

To compare novel-scaffold NRF2 activators to extant naphthalene-based activators, we were interested in studying the physical properties of these molecules beyond potency. There have been some recent perspectives that suggest that the emphasis of medicinal chemists, particularly those in academia, on potency often leads to highly potent, but poorly drug-like, molecules.[38] With these concerns in mind, we designed and synthesized compounds with scaffolds to replace the naphthalene as a means to study potency, aqueous solubility, metabolic stability and mutagenicity of NRF2 activators. Our results indicate that a 1,4-substituted isoquinoline presents a new scaffold for NRF2 activators that shows similar potency, aqueous solubility, and metabolic stability to the 1,4-substituted naphthalene. Additionally, a mini-Ames assay shows that the 1,4-substituted isoquinoline displays an improved mutagenic profile relative to the 1,4-substituted naphthalene. These results have important implications for the design of future NRF2 activators.

Results:

Analog Design.

NRF2 activators displaying a large set of different cores were synthesized based off the naphthalene compound **6a**. In previous work, we and others reported compounds varying the terminal rings, the sulfonamide R groups, the sulfonamide linker, and possible isosteric replacements for the carboxylates.[1, 29, 30] Additionally, we reported that the 1,4-substitution pattern was optimal, as other substitution patterns showed complete loss of activity. In the current work of designing non-naphthalene derivatives, we maintained the sulfonamides, either unsubstituted or with bis-carboxymethyl substitutions, and we varied the connecting scaffold. Previously, we showed that bis-carboxamide **6b** showed high potency.[1] During the course of the current studies, we determined that the amides of **6b** hindered aqueous solubility and caused rapid degradation in liver microsomes. As a result, we did not pursue this substituent in the current study.

We sought to synthesize compounds that maintained a display of substituents that was similar to that of the naphthalenes. To accomplish this, we synthesized molecules that featured a retention of the topology of the naphthalene that displayed different electronics (i.e., 1,4-isoquinoline; 5,8-quinoline; 1,4-phthalazine; 4,7-indole) (Figure 2). We also synthesized compounds that no longer contained the 6,6-fused ring system to examine the distal ring and possibilities of altering it (i.e., 1,4-benzene; 2,5-pyridine; o-xylene; 3,5-biphenyl; phthalamide). Lastly, we synthesized compounds that no longer contained an aromatic scaffold to fully determine what was necessary for activity (i.e., butene).

Analog Synthesis.

Compounds **5, 6a, and 6b** were synthesized as previously described.[1]

Benzenes **9b** and **11b** and di-substituted pyridine **11a** were synthesized (Scheme 1) starting from the reaction of phenylene-1,4-diamine **7b** or 2,5-diamino pyridine **7a** and *p*-methoxybenzenesulfonyl chloride **8** in pyridine to obtain the corresponding sulfonamides **9a** and **9b**. Reaction with ethyl bromoacetate in the presence of K_2CO_3 followed by saponification gave **11a** and **11b**.

Analogs with a 1,4-isoquinoline core were synthesized according to Scheme 2. 1-hydroxyisoquinoline **12** was converted to 1,4-dibromoisoquinoline **13** using PBr_5. An Ullmann-type coupling with *p*-methoxybenzenesulfonamide **14**, followed by alkylation and saponification yielded isoquinoline **17**. In the synthesis of isoquinoline **17**, undesired alkylation of the isoquinoline ring nitrogen, rather than the desired sulfonamide alkylation, could have occurred while installing the carboxymethyl functionalities (i.e **15** → **16**). 2D-NMR experiments confirmed the assigned sites of alkylation (Figure S8).

Compounds with a quinoline core were synthesized as shown in Scheme 3. 5-Aminoquinoline **18** was reacted with HONO in the presence of aniline to form the diazo compound **19**, which was further reduced in the presence of stannous chloride to yield 5,8-diaminoquinoline **20**.[39] Sulfonylation followed by alkylation and saponification yielded quinoline **23**.

Analogs containing an indole core were synthesized as shown in Scheme 4. 2,4-Difluoronitrobenzene **24** was sequentially aminated at the 2- and 4-positions to yield a differentially bis-aminated intermediate **25**. Cyclization was carried out in the presence of TFA to yield 4-benzylamino-7-nitroindole. Reduction and hydrogenolysis yielded 4,7-diaminoindole **26**,[40] which was further sulfonylated, alkylated, and saponified to yield indole **29**. HNMR results confirmed that compound **27** was sulfonylated at the 1- and 4-positions. Singlets at 10.69, 9.79, and 9.61, each integrating to 1H, correspond to the indole NH, and two sulfonamide NH groups.

Phthalazine **34** was prepared beginning from phthalonitrile **30**, which was condensed with hydrazine in methanol to give 1,4-diaminophthalazine **31**, which yielded the sulfonamide **32**. Alkylation of the sulfonamide gave only the mono-alkylated products **33** and **34**, regardless of the reaction conditions employed.

Analogs of **6a** that did not feature a fused ring system were synthesized using the appropriate electrophilic starting materials (Scheme 6). Substituted sulfonamides were used as nucleophiles to yield xylene **38**, phthalamide **40**, and butene **42** after saponification.

Biphenyl **46** was synthesized as shown in Scheme 7. 1-bromo-3,5-dinitrobenzene **43** was reacted with phenylboronic acid via a Suzuki coupling to create the biphenyl core. The nitro groups were reduced to amines to yield a diamino intermediate **44**, which was then sulfonylated, alkylated, and saponified to arrive at the analog **46**.

In vitro assays.

The IC_{50} of each compound for inhibiting the interaction of a fluorescent NRF2 peptide and the Kelch domain of KEAP1 was determined using fluorescence anisotropy.[41] The results are shown in Table 1. The heterocyclic cores ranged in potency: the 1,4-isoquinoline **17** (IC_{50} = 60 nM) retained much of the potency of the parent naphthalene **6a**, the 5,8-quinoline **23** was well tolerated (IC_{50} = 101 nM), the phthalazine **34** was tolerated (IC_{50} = 1000 nM), and the indole **29** was tolerated (IC_{50} = 1300 nM). Unfortunately, the indole **29** was found to be unstable, which precluded its further consideration. The non-fused systems all showed little to no activity: the phenyl **11b** was tolerated (IC_{50} = 980 nM), whereas the xylene **38**, pyridine **11b**, phthalamide **40**, and biphenyl **46** were all inactive (>25 μM). The removal of the core to give butene **42** also produced an inactive compound.

Compounds with low IC_{50} values in the FP assay were confirmed using an orthogonal Surface Plasmon Resonance (SPR) assay (Table 1). 1,4-Isoquinoline **17** exhibited a K_d of 102 nM, 5,8-quinoline **24** exhibited a K_d of 103 nM, and phthalazine **34** exhibited a K_d of >10 μM, in good agreement with the results of the FP assay.

Aqueous Solubility.

The aqueous solubility of all compounds at pH 7.4 was determined as shown in Table 2. Heterocycles **23** and **17**, phthalamide **40**, and butane **42** all showed solubility comparable to the naphthalene parent compound **6a**. Xylene **38** and benzene **11b** showed poor solubility. Pyridine **11b** and biphenyl **46** both showed moderate solubility. In all cases except

phthalazine **32**, unsubstituted sulfonamides were poorly soluble (solubility < **10** μM). The bis-amide **6b** that we previously reported as a potent NRF2 activator was shown to have poor solubility, which, in part, led us to focus our attention on the carboxymethyl analogs.

NRF2 Stabilization and NRF2 Target Gene Activation.

To see the effects of KEAP1 inhibitors on NRF2 activation, we carried out a screening assay to determine the effects of naphthalene acid **6a**, naphthalene amide **6b**, isoquinoline **17**, quinoline **23**, and phthalazine **34** on NRF2 protein stability and its downstream target gene activation in non-transformed immortalized human keratinocytes (HaCat cells). Cells were treated with compounds for 6 h to determine the stabilization of NRF2 and the protein expression levels of NQO1, a well-known target of NRF2 (Figure 3). Treatment of HaCaT cells with **6a**, **6b**, and **23** for 6 h caused a modest increase in protein levels of NRF2 and NQO1 expression in a manner comparable to CDDO-Im **1**, a well-known potent electrophilic activator of NRF2. Phthalazine **34** caused no increase in either NRF2 protein levels or NQO1 protein levels in this assay.

We next analyzed NRF2 and NQO1 protein expression levels in HaCat cells treated with compounds for a prolonged period (i.e., 24 h). Increased protein levels of NRF2 and NQO1 were noted in cells treated with naphthalene acid **6a**, naphthalene amide **6b**, or isoquinoline **17** for 24 h compared to vehicle-treated counterparts (Figure 3). Likewise, both NRF2 and NQO1 protein levels were higher in cells treated with CDDO-Im **1**. Quinoline **23** had no effect on either NRF2 stability or NQO1 expression. We also analyzed the expression of GCLM, a well-established target of NRF2. GCLM protein levels were significantly higher in cells treated with naphthalene acid **6a**, naphthalene amide **6b**, isoquinoline **17**, or CDDO **1** compared to vehicle controls. Unlike NRF2 protein stabilization or NQO1 protein expression, GCLM protein expression was modestly increased in cells treated with quinoline **23**.

Positive results in the screeening assay seen with isoquinoline **17** and quinoline **23** led us to examine nuclear accumulation of NRF2 (immunoblot) and expression of other NRF2 target genes (qPCR) in HaCaT cells treated with isoquinoline **17** and quinoline **23** at both 6 and 24 hour time points. NRF2 accumulation in the nucleus was increased two-fold when treated with isoquinoline **17** compared to DMSO control at both time points analyzed (Figure 4). A small significant increase in NRF2 nuclear accumulation was observed in cells treated with quinoline **23** at both time points. Analysis of mRNA levels in the HaCaT cells at 6 hours showed isoquinoline **17** produced a significant increase in *HMOX1*, *GCLM*, and *GCLC* mRNA expression (Figure 5). Isoquinoline **17** also produced an increase in *NQO1* mRNA expression at 24 hours. Quinoline **23** produced a small increase in *NQO1*, *GCLM*, and *GCLC* mRNA expression at 6 and 24 hours, with no increase observed for *HMOX1* mRNA expression. mRNA expression for *SOD* was also measured. *SOD* is not an NRF2 target gene, so, as expected, neither isoquinoline **17** nor quinoline **23** produced a significant increase in *SOD* expression. Western blot analysis of NQO1 protein levels corroborated the mRNA expression levels by showing a modest increase in protein expression in comparison to DMSO for both isoquinoline **17** and quinoline **23** (SI Figure S11).

Metabolic Stability in Liver Microsomes.

Active and moderately active compounds that showed good solubility were subjected to human and mouse liver microsomes for 20 minutes to ascertain the metabolic stability of the compounds. 1,4-Isoquinoline **17**, naphthalene **6a**, and 5,8-quinoline **23** were stable at 20 minutes in both human and mouse liver microsomes (Figure 6). Phthalazine **34** and 5,8-quinoline **23** showed reduced stability in human liver microsomes, but were comparable to the other compounds in mouse liver microsomes. The naphthalene amide **6b** was metabolically unstable, showing 0% compound remaining after 20 minutes in both mouse and human liver microsomes, providing further evidence that amide analogs may be rapidly hydrolyzed. The unsubstituted naphthalene **5** was metabolically unstable in mouse liver microsomes, showing only 15% remaining after 20 minutes.

Mutagenicity in a Mini-Ames Assay.

To probe our hypothesis that the naphthalene may prove to be mutagenic, we submitted naphthalene **6a** and isoquinoline **17** to a mini-Ames assay in *Salmonella typhimurium* and *Escherichia coli*. The compounds were tested for their ability to induce reverse mutations at the histidine locus of strains of *Salmonella typhimurium* (TA98, TA100, TA1535, TA1537) and *Escherichia coli* (WP2 uvrA (pKM101)) in the presence and absence of exogenous metabolic activation (Aroclor 1254 induced rat liver S9). Both naphthalene **6a** and isoquinoline **17** were screened at concentrations of 1.5, 4, 10, 25, 64, 160, 400 and 1000 μg/well. No cytotoxicity was observed in either naphthalene **6a** or isoquinoline **17** at any dose level. Naphthalene **6a** induced > 3-fold increases (for TA1535) and > 2-fold increases (for TA98 and TA100) that were statistically significant at higher dose levels in the presence of S9 mix, compared to vehicle control (Figure 7). Dose response was also observed in **6a** for TA98 and TA100; therefore, naphthalene **6a** was judged to be positive for mutagenicity. On the other hand, isoquinoline **17** induced a > 2-fold increase in only one strain (for TA98) at the highest dose level compared to the vehicle control. No dose response was observed for isoquinoline **17** (Figure 7). Taken together, these data lead us to conclude that isoquinoline **17** has a better mutagenic profile than naphthalene **6a**.

Discussion:

Previously, our lab investigated the structure-activity relationship of the distal substitutions on the naphthalene-based NRF2 activator **5**. We found that an electron-donating group on the terminal phenyl groups resulted in the most potent inhibitors. We also found that the sulfonamide linkages were superior to similar linkages and that substituting anything other than a carboxymethyl group or carboxamidomethyl group off the sulfonamide also resulted in an inactive compound.

Having explored the rest of the molecule, we turned our attention to the naphthalene scaffold. While there are drugs, including propranolol, that contain a naphthalene core, naphthalenes have been identified as a minor mutagenic scaffold in the Ames Mutagenicity Tree.[36] A related naphthalene **4**, RA-839, showed in vivo activity only if Phase 1 metabolism were blocked. Although the identity of the RA-839 metabolites are unknown, they may include reactive intermediates, as naphthalenes are known to be metabolically

activated to reactive naphthalene oxides and naphthoquinones. [32–35] With these points in mind, we explored alternative scaffolds.[31]

Our previous results suggested that compounds with amide-containing sidechains (e.g., **6b**) were comparable in potency to those containing carboxylic acid-containing sidechains.[1] During the course of the present study, however, we found that the amides are both relatively insoluble in water and metabolically unstable in liver microsomes, compared to the acids. This is in good agreement with work reported by Lu et al., who showed that amide-containing compounds were less soluble than acid-containing compounds at pH 7.4.[30] Because we were interested in compounds that would show good solubility and metabolic stability, we synthesized scaffolds that were decorated with *N*-carboxymethyl groups.

To probe the necessity of a 6,6-fused ring system, we synthesized non-fused rings and substitutions that might afford a disposition of substituents similar to the naphthalene scaffold. These substitutions included butene **42**, 1,4-substituted pyridine **11a**, 1,4-substituted benzene **11b**, 1,3,5-substituted benzene **46**, o-xylene **38**, and phthalamide **40**. Of these, only the benzene **11b** showed activity in the fluorescence anisotropy assay, albeit at values ca. 40-fold higher than the parent naphthalene **6a**. These compounds displayed varying levels of solubility that did not divulge any discernible pattern. The butene **42** and phthalamide **40** showed solubilities similar to the parent naphthalene **6a**, the pyridine **11a** and 1,3,5-substituted benzene **11a** showed slight solubility, and the o-xylene and 1,4-substituted benzene **11b** proved insoluble. Because these compounds showed poor potency and solubility comparable to other scaffolds, we did not carry them into liver microsome stability studies.

To probe the necessity of the all-carbon framework of the naphthalene scaffold, we replaced the naphthalene core with nitrogen-containing heterocycles, including 1,4-phthalazine **34**, 1,4-isoquinoline **17**, 5,8-quinoline **23**, and 4,7-indole **29**. Of these, 5,8-quinoline **23** and 1,4-isoquinoline **17** retained good potency in both FP (IC$_{50}$ = 101 and 60 nM, respectively) and SPR assays (K_d = 103 and 102 nM, respectively). The 1,4-phthalazine **34** scaffold was less potent (IC$_{50}$ = 1000 nM; K_d >10 μM). Previously, we reported that a naphthalene mono-acid showed good affinity for KEAP1 (IC$_{50}$ = 61 nM).[1] Phthalazine **34**, which is also a mono-acid, is less potent than the naphthalene mono-acid, but this is in agreement with the affinity of the unsubstituted cores: unsubstituted naphthalene **5** has an IC$_{50}$ of 0.96 μM, while the unsubstituted phthalazine **32** has an IC$_{50}$ of > 25μM. Taken together, these data suggest that the all-carbon framework of the naphthalene is not necessary for binding to KEAP1, and other 6,6-fused systems can be used to replace the naphthalene scaffold.

The binding of this class of compounds is dictated, in part, by a π-cation interaction between the π-system of the inhibitor and Arg415, first observed by Marcotte et al.[27] Dougherty and coworkers have comprehensively studied the binding energy of cations to a number of different π-systems. Their work suggests that electron-rich systems, like indole, should be better cation binders than naphthalene, which should be better than electron-poor systems like quinoline and isoquinoline.[42–44] In our work, we see that substituted and unsubstituted naphthalenes **5** and **6a** show a slightly higher affinity than the corresponding quinolines (**21** and **23**) and isoquinolines (**17**), which is consistent with this ordering (Table 1). On the other

hand, indoles **27** and **29** show an IC_{50} of >25 μM and 1300 nM, while naphthalene **5** shows an IC_{50} of 960 nM. While the instability of the indole-containing di-acid may complicate this analysis, these data may suggest that the contribution of the π-cation interaction to binding may be offset by other factors. Additional analogs and future experiments may shed more light on these intriguing observations.

With two charged carboxylates, naphthalene **6a** shows high aqueous solubility at pH 7.4 (440 μM). These high solubility values are maintained across most of the heterocyclic scaffolds, as well. The carboxylates clearly contribute to the solubility, as the unsubstituted compounds **5**, **9b**, and **15** show only modest aqueous solubilities.

The stabilities of these compounds in mouse and human liver microsomes suggest that the most metabolically stable compounds are naphthalene **6a**, 1,4-isoquinoline **17**, and 5,8-isoquinoline **23**. After 20 minutes of incubation with mouse or human liver microsomes, there was little loss of compound. This is in contrast to the bis-amide **6b** and the unsubstituted compound **5**, which were both rapidly degraded in this time frame. This is in good agreement with a previous report that naphthalene **4** (Chart 2), which is alkylated on only one aromatic nitrogen, is metabolized quickly in vivo.[31] These data suggest that several 1,4-diamino scaffolds are stable, as long as both nitrogen atoms are alkylated. Further evidence for this point comes in the metabolic stability data for phthalazine **34**, with approximately 50% of the compound remaining after 20 minutes of incubation with human liver microsomes. The mono-carboxylate system presents its own advantages over the bis-carboxylate system; the overall charge of the molecule is lessened which may assist in cell permeability. The current results suggest, however, that the substitution pattern may play a major role in the metabolic stability of the molecules, which may imply that a balance is needed between charge state and substitution.

Our results obtained from immunoblot analysis demonstrate NRF2 stabilization and transactivation of its target gene expression by compounds **6a**, **6b**, or **17** in human keratinocytes in a manner comparable to CDDO **1**, a potent activator of NRF2. The effects of these compounds were more pronounced at 24 h, although they showed a modest effect on NRF2 stabilization and NQO1 expression when treated for a shorter period (6 h). CDDO **1** had a similar effect on NRF2 and its target gene activation in HaCat cells. Previously, we have shown increased protein levels of NRF2 stabilization and its target gene activation by NRF2 activator compounds in lung epithelial cells at 6h-post treatment.[1] A robust increase in NRF2 stabilization and the induction of NRF2 target gene expression in HaCat cells by the activators at 24 h but not at 6 h post-treatment could be attributable to cell-specific effects, as CDDO **1**, a potent NRF2 activator, also showed a similar activation pattern in HaCat cells. Nonetheless, our studies showed **6a**, **6b**, and **17** activate NRF2 target gene expression in human keratinocytes in a manner comparable to CDDO **1**.

Our immunoblot analysis led us to measure nuclear accumulation of NRF2 and NQO1 in conjunction with mRNA expression of NRF2 target genes in HaCaT cells treated with isoquinoline **17** and quinoline **23** (Figure 5). The results showed that treatment with isoquinoline **17** produced a 2-fold increase of NRF2 accumulation in the nucleus at 6 and 24 hours along with a corresponding increase in NRF2 target genes *NQO1*, *HMOX1*, *GCLM*,

and *GCLC*. Treatment with quinoline **23** showed a modest increase of NRF2 accumulation in the nucleus at 6 and 24 hours with a small increase in NRF2 target genes *NQO1*, *GCLM*, and *GCLC*. No increase in *HMOX1* was observed in cells treated with quinoline **23**.

Even though quinoline **23** showed good affinity for KEAP1 and activated NRF2 target genes, it was not completely stable to human liver microsomes, with 50% remaining after 20 minutes. We are uncertain of the identities of the metabolites, but, taken together with the potential for an 8-aminoquinoline scaffold to chelate metals, these data suggest that this scaffold should be deprioritized.

A mini-Ames assay conducted on naphthalene acid **6a** and isoquinoline **17** showed that neither compound is cytotoxic, but the data collected led us to conclude that isqouinoline **17** showed a better mutagenic profile than naphthalene **6a**. Naphthalene **6a** induced > 2-fold increases and > 3-fold increases of reverse mutations at the histidine locus of three strains of *Salmonella typhimurium* (TA98, TA100, TA1535) in a dose-dependent manner. Isoquinoline **17** induced a > 2-fold increase of reverse mutations at the histidine locus of *Salmonella typhimurium* strain TA98 at only the highest dose, with no dose-response observed. These data demonstrated that isoquinoline **17** had a better mutagenic profile than naphthalene **6a** and should be studied more closely.

Generally, the compounds' abilities to activate NRF2 target genes correlated with *in vitro* potency, solubility, and metabolic stability, as naphthalene **6a**, isoquinoline **17**, and quinoline **23** all showed good *in vitro* potency and solubility, as well as varying degrees of metabolic stability. An exception is the bis-amide **6b**, which was metabolically unstable and poorly soluble but able to activate NRF2 target genes. It is possible that one or both of the amides are hydrolyzed to acids (e.g., **6a**) in cell culture, which may produce its activation of NRF2 target genes. The neutrally charged amides may support cell permeability, similar to the effect we have previously reported for an ester,[1] but the poor aqueous solubility of amide **6b** suggests that a primary amide is a poor mask of the acid for optimization of these compounds. You and coworkers have previously reported that isosteres of carboxylic acids are soluble, cell-permeable, and supportive of NRF2-regulated gene activation.[30] Taken together with our data, these results suggest that an isostere or prodrug approach may be a good strategy for multi-parameter optimization of this class of molecules.

Indeed, it is likely that the bis-acid substitution pattern is not optimal for development of a preclinical candidate.[45] We are working to reduce the number of carboxylic acids contained in the 1,4-isoquinoline scaffold. These compounds need further optimization and verification if their effects are to be translated to clinical trials, but they present a promising strategy for developing Nrf2 activators.

The two compounds that show high affinity, stability and solubility are naphthalene **6a** and 1,4-isoquinoline **17**. These compounds show stabilization of NRF2 and activation of NRF2 target genes in western blots as well. While much work has been done by us[1] and others[28, 30, 46] on the substituents on the naphthalene scaffold, the current work has identified 1,4-isoquinoline as a new scaffold for optimizing noncovalent NRF2 activators, a

topic of considerable current research activity. We foresee that the 1,4-isoquinoline core may provide a number of advantages relative to naphthalene.

First, the naphthalene scaffold may be more toxic and/or mutagenic than the isoquinoline scaffold. Oral toxicity as predicted by PROTOX, an online prediction tool that works through analysis of a structure and comparison to known toxicophores and toxic fragments, [47] predicted the naphthalene **6a** to be slightly toxic in the class of 4/6 whereas the 1,4-isoquinoline **17** was predicted to be non-toxic in the class 6/6. Lazar toxicity predictions, which generate QSAR models for compounds to predict toxicity,[48] mirrored this by predicting the 1,4-isoquinoline **17** to be less toxic than the naphthalene **6a** across all categories calculated. Beyond these computational studies, we have conducted a mini-Ames assay on naphthalene **6a** and isoquinoline **17**, the latter of which was shown to be less mutagenic than naphthalene **6a**.

Second, the unsymmetrical nature of the 1,4-isoquinoline serves to desymmetrize the molecule. The binding site on KEAP1 is not symmetrical, and we and others have shown that symmetrical ligands are not required for binding to KEAP1;[24, 46] the current work further emphasizes that point.

Lastly, the pharmacokinetics of a negatively charged NRF2 activator may be enhanced by the presence of a basic nitrogen. In support of this, we experimentally determined the $\text{LogD}_{7.4}$ values of naphthalene **6a** (−1.9) and 1,4-isoquinoline **17** (−1.7). The slight improvement in $\text{LogD}_{7.4}$ seen with isoquinoline **17** suggests this scaffold may provide a better starting point for further optimization of these molecules.

Overall, there have been a number of medicinal chemistry and biological studies that have been carried out using naphthalene-based NRF2 activators.[1, 28, 30, 31, 49, 50] Our data suggest that it may be prudent to consider other scaffolds going forward.

Conclusion

In conclusion, this work demonstrates that the naphthalene core of non-electrophilic NRF2 activators may be replaced with 1,4-isoquinoline, with little to no disadvantage in potency, cellular activity, solubility or metabolic stability. Importantly, isoquinoline **17** displays a better mutagenic profile than naphthalene **17**. Other heterocycles and scaffolds were examined, as well, but each of these had at least one liability that isoquinoline **17** did not have. We have also shown that alkylation of the sulfonamide nitrogens in this series is necessary for metabolic stability in liver microsomes. Taken together, these data suggest that, relative to the often-used naphthalene scaffold, isoquinoline **17** represents a preferable core for new NRF2 activators.

Experimental

Chemistry:

General considerations.—^{1}H and ^{13}C NMR spectra were recorded on a Bruker AVIII and AVIII HD 400 spectrometers equipped with a room temperature 5 mm broadband

observe (BBO) probes with z-gradient. Chemical shifts were reported in parts per million (δ) using either tetramethylsilane (TMS) or the undeuterated residual solvent peak as an internal standard (CDCl$_3$: ^{1}H δ = 7.26 and ^{13}C δ = 77.2; CD$_3$COCD$_3$: ^{1}H δ = 2.05 and ^{13}C δ = 29.2; CD$_3$OD: ^{1}H δ = 3.31 and ^{13}C δ = 49.2; CD$_3$CN: ^{1}H δ = 1.96and ^{13}C δ = 118.3; DMSO-d_6: ^{1}H δ = 2.50 and ^{13}C δ = 39.5). Purity of each of the final, tested compounds was determined by HPLC on a Shimadzu LC-20AB (Solvent system; MeCN/H$_2$O, 0.1% Formic Acid; Column: Shimadzu C18, 50 μm, 50 × 4.6 mm) and was   95% (HPLC Method: 15:85 MeCN:H$_2$O, 0–2 min; 15:85 – 95:5 MeCN:H$_2$O, linear gradient, 2 – 9 min; 95:5 MeCN:H$_2$O, 9–10.7 min; 95:5 – 15:85 MeCN:H$_2$O, linear gradient, 10.7 – 11 min; 15:85 MeCN:H$_2$O, 11 – 13 min. UV, 254 nm). The HRMS spectra were recorded on a Shimadzu LCMS-IT-TOF. Flash chromatography was performed on a Teledyne-Isco Combiflash Rf+ system using preloaded silica gel cartridges (230–400 mesh). Reactions were monitored by thin-layer chromatography (TLC) on silica gel GHLF plates (250 μm, Macherey-Nagel, Inc.).

N,N'-(pyridine-2,5-diyl)bis(4-methoxybenzenesulfonamide) (9a)—This previously unreported compound was synthesized in a manner similar to a published procedure.[1] 2,5-diaminopyridine dihydrochloride **7a** (3.0 g, 1.0 eq, 16.47 mmol) was dissolved in a mixture of THF (18 mL) and pyridine (6 mL). The mixture was heated to reflux and allowed to stir for a half hour. 4-methoxybenzenesulfonyl chloride **8** (8.16 g, 2.4 eq, 39.52 mmol) was added, and the reaction mixture stirred for 18 hours at reflux. The reaction was monitored by TLC (3:1, ethyl acetate:hexanes) and, upon completion, was quenched with ice water. The precipitate was filtered and washed with methanol. The product **9a** was obtained as a white solid (1.5 g 18% yield). ^{1}H NMR (400 MHz, DMSO-d_6, δ): 10.8197 (br.s, 1H), 10.04 (s, 1H), 7.68–7.83 (m, 3H), 7.58 (d, J = 8.93 Hz, 2H), 7.39 (dd, J = 2.71, 8.85 Hz, 1H), 6.95–7.13 (m, 5H), 3.81 (s, 3H), 3.80 (s, 3H)

N,N'-(1,4-phenylene)bis(4-methoxybenzenesulfonamide) (9b)—This previously unreported compound was synthesized in a manner similar to a published procedure.[51] A solution of p-aminoaniline (0.5 g, 4.6 mmol) and p-methoxybenzenesulfonyl chloride (2.4 g, 11.6 mmol) in pyridine (3–5 mL) was allowed stir at room temperature for 24 h. On completion, the reaction mixture was diluted with EtOAc (40 mL), washed with H$_2$O (2 × 50 mL) and HCl (2N, 2 × 50 mL), dried over Na$_2$SO$_4$, and evaporated to yield the crude product, which, upon recrystallization from EtOH, yielded 1.6 g (76% yield) of (**9b**) as white needles. ^{1}H NMR (400 MHz, DMSO-d_6, δ): 9.93 (s, 2H), 7.49–7.66 (AA'XX', J = 8.8 Hz, 4H), 6.96–7.09 (AA'XX', J = 8.8 Hz, 4H), 6.90 (s, 4H), 3.79 (s, 6H); ^{13}C NMR (100 MHz, DMSO-d_6, δ): 162.4, 134.1, 131.1, 128.9, 121.5, 114.3, 55.7; HRMS-ESI (−) (m/z): [M-H]$^-$ calcd for C$_{20}$H$_{20}$N$_2$O$_6$S$_2$, 447.0685; found, 447.0696.

Diethyl 2,2'-(pyridine-2,5-diylbis((4-methoxyphenyl)sulfonyl)azanediyl))diacetate (10a)—This previously unreported compound was synthesized in a manner similar to a published procedure.[1] **9a** (0.700 g, 1.0 eq, 1.40 mmol) was dissolved in DMF (10 mL). Potassium carbonate (K$_2$CO$_3$, 0.445 g, 2.3 eq, 3.22 mmol) was added, and the mixture was stirred for a 0.5 hour at room temperature. Ethyl bromoacetate (340 μL, 2.2 eq, 3.08 mmol) was added, and the reaction mixture stirred for 16 hours at room temperature. The reaction was monitored by TLC (3:1, ethyl

acetate:hexanes) and, upon completion, ice water was added to the mixture, whereupon a precipitate formed. The precipitate was filtered and recrystallized from ethanol to yield 0.702 g (80% yield). ^{1}H NMR (400 MHz, DMSO-d_6, δ): 8.09 (d, J = 2.5 Hz, 1H), 7.70 (dd, J = 2.0, 6.8 Hz, 2H), 7.62 (dd, J = 2.0, 6.9 Hz, 2H), 7.54 (dd, J = 2.6, 9.8 Hz, 1H), 7.32 (d, J = 9.8 Hz, 1H), 7.10 (dd, J = 2.0, 7.0 Hz, 2H), 7.03 (dd, J = 2.0, 6.9 Hz, 2H), 4.91 (s, 2H), 4.37 (s, 2H), 4.09 (m, 4H), 3.86 (s, 3H), 3.81 (s, 3H), 1.14 (m, 6H).

2,2'-(pyridine-2,5-diylbis(((4-methoxyphenyl)sulfonyl)azanediyl))diacetic acid (11a)—This previously unreported compound was synthesized in a manner similar to a published procedure.[1] **10a** (0.200 g, 1.00 eq, 0.319 mmol) was dissolved in a solution of 15% sodium hydroxide (NaOH, 20 mL), and methanol (MeOH, 20 mL) was added to this. The reaction mixture was stirred at reflux for 8 hours. The reaction was monitored by TLC (3:1, ethyl acetate:hexanes) and, upon completion, the mixture was concentrated *in vacuo*. The aqueous mixture was acidified to a pH of ~6.0. On formation of precipitate, the flask was placed in a 4 °C refrigerator. The precipitate was then filtered and washed with diethyl ether to yield 0.180 g of a white solid (66% yield). ^{1}H NMR (400 MHz, DMSO-d_6, δ): 13.07 (b.s., 2H), 8.05 (d, J = 2.3 Hz, 1H), 7.71 (d, J = 8.8 Hz, 2H), 7.59 (d, J = 8.9 Hz, 2H), 7.55 (dd, J = 2.4, 9.7 Hz, 1H), 7.28 (d, J = 9.8 Hz, 1H), 7.07 (d, J = 8.9 Hz, 2H), 7.00 (d, J = 8.8 Hz, 2H), 4.84 (s, 2H), 4.25 (s, 2H), 3.85 (s, 3H), 3.81 (s, 3H). ^{13}C NMR (400 MHz, DMSO-d_6, δ): 169.9, 168.4, 163.5, 161.9, 154.6, 143.0, 142.2, 135.7, 130.1, 129.4, 128.4, 124.3, 116.2, 115.1, 114.3, 56.2, 55.9, 54.2, 51.8 HRMS–ESI (+) (*m/z*): [M+H]$^+$ calcd for $C_{23}H_{23}N_3O_{10}S_2$; 565.0892, found: 565.0825.

2,2'-(1,4-phenylene)bis(((4-methoxyphenyl)sulfonyl)azanediyl))diacetic acid (11b)—This previously unreported compound was synthesized in a manner similar to a published procedure.[28] Potassium carbonate (0.28 g, 2.01 mmol) and ethyl bromoacetate (0.23 g, 1.4 mmol) were added to a solution of **9b** (0.3 g, 0.67 mmol) in anhydrous DMF (2 mL), and the reaction was stirred at room temperature for 3 h. On completion the reaction was quenched with H_2O (25 mL) and acidified with HCl (2N, to pH 3). The precipitate was collected by filtration and dried. A fraction of the dried product **10b** (0.1 g) was suspended in NaOH (10%, 5 mL) and MeOH (10 mL) and allowed to reflux for 2 h. On completion the reaction mixture was cooled, the organic portion was evaporated, and diluted with H_2O (20 mL) and HCl (2N, to pH 3) to yield a white-colored precipitate. The crude was recrystallized from MeOH to yield 0.06 g (67% yield) of **11b** as a white-colored solid. ^{1}H NMR (400 MHz, DMSO-d_6, δ): 12.86 (br s, 2H), 7.53 (d, J = 8.8 Hz, 4H), 6.97–7.19 (m, 8H), 4.36 (s, 4H), 3.84 (s, 6H); ^{13}C NMR (100 MHz, DMSO-d_6, δ): 170.3, 163.2, 139.1, 130.2, 129.9, 128.1, 114.7, 56.2, 52.2; HRMS-ESI (–) (*m/z*): [M-H]$^-$ calcd for $C_{24}H_{24}N_2O_{10}S_2$, 563.0794; found, 563.0596.

1,4-dibromoisoquinoline (13)—This previously reported compound was synthesized according to a published procedure.[52] In a 50 mL round bottom flask, isocarbostyril (0.50 g, 3.4 mmol) and phosphorus tribromide (2.7 g, 9.8 mmol) were heated at 140–145 °C for 10 min. The solid melted and lightened in color. The liquid solidified, and the reaction was stirred for an additional 10 min. On completion, the reaction mixture was cooled to room temperature, and ice/H_2O (10 mL) was poured into the flask. The buff-colored solid was

collected by filtration and washed with H_2O (2×50 mL) and dried under vacuum to obtain **13** (0.86 g, 89% yield) as a buff-colored solid. ^{1}H NMR (400 MHz, CDCl$_3$, δ) 8.45 (s, 1H), 8.33 (d, $J = 8.8$ Hz, 1H), 8.19 (d, $J = 8.4$ Hz, 1H), 7.88 (t, 1H), 7.78 (t, 1H).

N,N'-(isoquinoline-1,4-diyl)bis(4-methoxybenzenesulfonamide) (15)—This previously unreported compound was synthesized in a manner similar to a published procedure.[53,54] A solution of 1,4-dibromoisoquinoline **13** (230 mg, 0.8 mmol), 4-methoxybenzenesulfonamide **14** (300 mg, 1.6 mmol), CuI (60 mg, 0.3 mmol), K_2CO_3 (1.18 g, 8.5 mmol), and N^1,N^2-dimethylethane-1,2-diamine (142 mg, 1.6 mmol) in MeCN (6 mL) was heated at 70 °C for 7 days. On completion the reaction mixture was quenched with H_2O (20 mL), and the yellow-colored solid was collected by filtration. The collected solid was washed with Et$_2$O (10 mL) and dried to yield 240 mg (60% yield) of **15** as a yellow-colored solid. ^{1}H NMR (400 MHz, DMSO-d_6) δ 8.62 (d, $J = 8.3$ Hz, 1H), 8.28 (d, $J = 8.4$ Hz, 1H), 7.86 (t, $J = 7.6$ Hz, 1H), 7.77 (t, $J = 7.7$ Hz, 1H), 7.66 (s, 1H), 7.64 – 7.58 (m, 2H), 7.48 – 7.42 (AA'XX', 2H), 7.14 – 7.08 (AA'XX', 4H), 3.88 (d, 6H). ^{13}C NMR (CD$_3$CN) δ 163.4, 162.6, 152.5, 135.5, 133.5, 132.5, 130.5, 129.5, 129.3, 128.6, 128.3, 128.0, 126.8, 122.7, 114.3, 114.1, 55.6, 55.4. HRMS-ESI (+) (*m/z*): [M+H]$^+$ calcd for $C_{23}H_{21}N_3O_6S_2$, 500.0945; found, 500.0940.

2,2'-(isoquinoline-1,4-diylbis(((4-methoxyphenyl)sulfonyl)azanediyl))diacetic acid (17)—This previously unreported compound was synthesized in a manner similar to a published procedure.[1] Potassium carbonate (83 mg, 0.6 mmol) and ethyl bromoacetate (70 mg, 0.4 mmol) were added to a solution of N,N'-(isoquinoline-1,4-diyl)bis(4-methoxybenzenesulfonamide) **15**, (100 mg, 0.20 mmol) in anhydrous DMF (2 mL), and the reaction was stirred overnight at room temperature. On completion the reaction was quenched with H_2O (10 mL) and the solid was collected by filtration to yield a brown-colored solid which was subjected to saponification using NaOH (10%, 0.5 mL) and MeOH (2 mL) and allowed to reflux for 1.5 h. On completion the reaction mixture was cooled, and the organic portion was evaporated and diluted with H_2O (10 mL). The solid was removed by filtration, and the filtrate was acidified with HCl (2N, to pH 2) and extracted with EtOAc (2×5 mL). The combined organic portions were washed with H_2O (2×10 mL), dried (Na$_2$SO$_4$), and evaporated to yield a yellow solid as crude product (77% yield). 15 mg of the crude product was further purified by preperative HPLC (C18, 20–95% MeCN with 0.1% formic acid, 205 mL/min) to yield 5 mg of **17** as a buff-colored solid. ^{1}H NMR (400 MHz, DMSO-d_6, δ) 8.62 (d, $J = 8.4$ Hz, 1H), 8.28 (d, $J = 8.4$ Hz, 1H), 7.86 (t, $J = 7.6$ Hz, 1H), 7.77 (t, $J = 7.6$ Hz, 1H), 7.66 (s, 1H), 7.64 – 7.56 (AA'XX', 2H), 7.49 – 7.41 (AA'XX', 2H), 7.15 – 7.07 (AA'XX', 4H), 4.42 (s, 2H), 4.30 (d, $J = 31.7$ Hz, 2H), 3.88 (s, 3H), 3.87 (s, 3H). ^{1}H NMR (CD$_3$COCD$_3$, 400 MHz, δ) 8.81 (d, $J = 8.6$ Hz, 1 H), 8.31 (d, $J = 8.3$ Hz, 1 H), 7.93 (s, 1 H), 7.84 – 7.91 (m, 1 H), 7.77 – 7.83 (m, 1 H), 7.70 – 7.75 (m, 2 H), 7.52 – 7.57 (m, 2 H), 7.09 – 7.18 (m, 4 H), 4.67 – 4.78 (m, 1 H), 4.48 – 4.64 (m, 3 H), 3.98 (s, 3 H), 3.96 ppm (s, 3 H) ^{13}C NMR (CD$_3$CN, δ): 170.4, 169.7, 164.7, 164.6, 153.5, 142.7, 138.2, 133.6, 132.5, 131.6, 131.1, 130.4, 129.6, 128.9, 128.8, 128.8, 124.2, 115.3, 115.2, 56.6, 56.6, 53.6, 52.1. ^{13}C NMR (CD$_3$COCD$_3$, 101 MHz, δ): 171.0, 170.1, 165.3, 165.2, 154.4, 143.7, 138.8, 134.1, 132.8, 132.3, 131.8, 131.8, 130.5, 130.0, 129.8, 129.0, 124.8, 115.8, 115.8, 57.0,

57.0, 54.3, 52.6 ppm; HRMS-ESI (+) (*m/z*): [M+H]$^+$ calcd for $C_{27}H_{25}N_3O_{10}S_2$, 616.1054; found, 616.1036.

(*E/Z*)-8-(phenyldiazenyl)quinolin-5-amine (19)—This previously unreported compound was synthesized in a manner similar to a published procedure.[55] In a 250 mL round-bottomed flask, aniline (1.0 g) was dissolved in HCl (1N, 30 mL), and the solution was chilled in an ice-bath (solution 1). NaNO$_2$ (0.76 g) was added and the reaction mixture was allowed to stir for 15 min. In a separate 250 mL round-bottomed flask, quinoline-5-amine **18** (1.5 g) was dissolved in AcOH (1N, 20 mL), NaOAc (saturated, 20 mL) and H$_2$O (200 mL) and chilled in an ice-bath below 10 °C (solution 2). Solution 1 was slowly added to solution 2 while maintaining the temperature below 10 °C, during which time the solution changed color from red to deep-red. After complete addition the reaction was allowed to stir for an additional 15 min and poured into NH$_4$OH (100 mL) and ice to obtain a red precipitate. The solid was collected by filtration and washed further with H$_2$O (300 mL) and recrystallized from EtOH/H$_2$O (50/50) to yield 0.8 g (30% yield) of **19** as deep-red needles. The product was utilized for the synthesis of **20** without further purification or characterization.

Quinoline-5,8-diamine (20)—This previously unreported compound was synthesized in a manner similar to a published procedure.[40] Tin chloride dihydrate (5.1 g, 22.6 mmol) was added to a solution of (*E/Z*)-8-(phenyldiazenyl)quinolin-5-amine **19** (0.7 g, 2.8 mmol) in conc. HCl (20 mL), and the reaction mixture was allowed to stir at reflux for 4 h. On completion the reaction was cooled in an ice-bath, and KOH was slowly added until a pH of 8–9 was attained. The solid was filtered and washed with EtOH (2 × 100 mL), and the organic portion was kept aside for slow evaporation to obtain 0.22 g (50% yield) of **20** as needles. ^{1}H NMR (400 MHz, DMSO-*d*$_6$, δ): 8.61–8.73 (m, 1H), 8.38 (d, *J* = 8.6 Hz, 1H), 7.27–7.42 (m, 1H), 6.72 (d, *J* = 7.8 Hz, 1H), 6.59 (d, *J* = 7.8 Hz, 1H), 5.03 (br. s, 2H), 4.96 (br. s, 2H).

N,N'-(quinoline-5,8-diyl)bis(4-methoxybenzenesulfonamide) (21)—This previously unreported compound was synthesized in a manner similar to a published procedure.[51] A solution of quinoline-5,8-diamine **20** (0.1 g, 0.6 mmol) and *p*-methoxybenzenesulfonyl chloride (0.27 g, 1.3 mmol) in pyridine (4 mL) was allowed to stir overnight at room temperature. On completion, the reaction mixture was diluted with EtOAc (40 mL); washed with H$_2$O (2 × 50 mL) and brine (50 mL); dried (Na$_2$SO$_4$); and evaporated to yield the crude product, which, upon recrystallization from *i*-PrOH, yielded 0.24 g (77% yield) of **21** as buff-colored needles. ^{1}H NMR (400 MHz, DMSO-*d*$_6$, δ): 10.05 (s, 1H), 9.81 (s, 1H), 8.80 (d, *J* = 4.0 Hz, 1H), 8.29 (d, *J* = 8.6 Hz, 1H), 7.80 (d, *J* = 8.6 Hz, 2H), 7.39 – 7.62 (m, 4H), 7.09 (d, *J* = 8.1 Hz, 1H), 6.96 (t, *J* = 9.4 Hz, 4H), 3.74 (s, 3H), 3.77 (s, 3H); ^{13}C NMR (100 MHz, DMSO-*d*$_6$, δ): 163.1, 162.9, 149.8, 139.3, 133.0, 132.9, 131.3, 131.2, 129.7, 129.4, 128.1, 125.7, 124.9, 122.5, 116.2, 114.7, 56.1; HRMS-ESI (+) (*m/z*): [M+H]$^+$ calcd for $C_{23}H_{21}N_3O_6S_2$, 500.0905; found, 500.0946.

2,2'-(quinoline-5,8-diyl)bis(((4-methoxyphenyl)sulfonyl)azanediyl))diacetic acid (23)—This previously unreported compound was synthesized in a manner similar to a

published procedure.[28] Potassium carbonate (0.07 g, 0.48 mmol) and ethyl bromoacetate (0.06 g, 0.35 mmol) were added to a solution of **21** (0.08 g, 0.16 mmol) in anhydrous DMF (2 mL), and the reaction was stirred overnight at room temperature. On completion the reaction was quenched with H_2O (25 mL), and the solid was collected by filtration, suspended in NaOH (10%, 5 mL) and MeOH (10 mL), and allowed to reflux for 2 h. On completion the reaction mixture was cooled, and the organic portion was evaporated and diluted with H_2O (20 mL). The solid was removed by filtration, and the filtrate was acidified with HCl (2N, to pH 6) and extracted with EtOAc (2 × 25 mL). The combined organic portions were washed with H_2O (3 × 50 mL) and brine (20 mL), dried (Na_2SO_4), and evaporated to yield a pastel green precipitate. The crude product was further recrystallized from MeOH to yield 0.06 g (67% yield) of **23** as a white solid. ^{1}H NMR (400 MHz, CD_3OD, δ): 12.86 (s, 1H), 8.51–8.74 (m, 2H), 7.69 (d, $J = 8.1$ Hz, 1H), 7.51 (d, $J = 8.8$ Hz, 2H), 7.56 (d, $J = 8.6$ Hz, 3H), 7.26 (d, $J = 8.1$ Hz, 1H), 7.11 (d, $J = 8.8$ Hz, 2H), 6.94 (d, $J = 8.8$ Hz, 2H), 4.63 (br s, 2H), 4.48 (s, 1H), 4.36 (d, 1H), 3.87 (s, 3H), 3.80 (s, 3H); ^{13}C NMR (100 MHz, DMSO-d_6, δ): 170.7, 169.0, 163.5, 163.0, 147.7, 138.3, 136.3, 135.8, 131.2, 130.6, 130.3, 129.4, 128.7, 114.8, 111.6, 56.2; HRMS-ESI (+) (*m/z*): [M+H][+] calcd for $C_{27}H_{26}N_3O_{10}S_2$, 616.1015; found, 616.1060.

N-(2,2-dimethoxyethyl)-5-fluoro-2-nitroaniline—This previously reported compound was synthesized according to a published procedure.[56] Diisopropylethylamine (4.4 mL, 13.2 mmol) and aminoacetaldehyde dimethyl acetal (3.3 mL, 30.2 mmol) were added to a solution of 2,4-difluoro-1-nitrobenzene (2.8 mL, 13.2 mmol) in MeOH (100 mL), and the reaction mixture was stirred at reflux for 15 h. On completion, the organic portions were evaporated, and the residue was dissolved in EtOAc (100 mL). The organic portion was washed with H_2O (2 × 100 mL) and brine (100 mL), dried (Na_2SO_4) and evaporated to yield 5.3 g (86% yield) of an orange oil. ^{1}H NMR (400 MHz, $CDCl_3$, δ): 8.28 (br s, 1H), 8.24 (dd, $J = 9.5, 6.2$, Hz, 1H), 6.53 (dd, $J = 11.4, 2.5$ Hz, 1H), 6.40 (ddd, $J = 9.5, 7.1, 2.8$ Hz, 1H), 4.65 (t, $J = 5.4$ Hz, 1H), 3.46–3.50 (m, 6H), 3.45 (d, 1H), 3.41 (t, $J = 5.4$ Hz, 2H).

N[1]-benzyl-N[3]-(2,2-dimethoxyethyl)-4-nitrobenzene-1,3-diamine (25)—This previously reported compound was synthesized according to a published procedure.[56] A solution of N-(2,2-dimethoxyethyl)-5-fluoro-2-nitroaniline (3 g, 12.3 mmol) and benzylamine (8 mL, 72.7 mmol) in 1,4-dioxane (15 mL) was stirred at reflux for 3 days. On completion, the reaction mixture was cooled to room temperature and diluted with EtOAc (80 mL). The mixture was washed with H_2O (3 × 100 mL) and HCl (2N, 2 × 75 mL), dried (Na_2SO_4), and evaporated to yield 3.8 g (93% yield) of **25** as an orange oil which solidified on standing. The product was taken directly to the next step without purification or characterization.

N-benzyl-7-nitro-1H-indol-4-amine—This previously reported compound was synthesized according to a published procedure.[56] A solution of N[1]-benzyl-N[3]-(2,2-dimethoxyethyl)-4-nitrobenzene-1,3-diamine (**25**, 3.7 g, 11.4 mmol) and TFA (6 mL) in CH_2Cl_2 (40 mL) was stirred overnight at room temperature. On completion, the reaction was quenched with H_2O (50 mL), and the aqueous layer was further extracted with CH_2Cl_2 (3 × 30 mL). The combined organic portions were washed with H_2O (3 × 100 mL), dried

(Na$_2$SO$_4$) and evaporated to yield a crude residue which was purified by column chromatography (silica gel; hexanes/EtOAc; 90:10 to 70:30) to afford 2.5 g (85% yield) of a dark orange solid. ^{1}H NMR (400 MHz, DMSO-d_6, δ): 11.61 (br. s, 1H), 8.19 (t, $J = 6.3$ Hz, 1H), 7.89 (d, $J = 9.1$ Hz, 1H), 7.28–7.41 (m, 4H), 7.16–7.28 (m, 2H), 6.94 (d, $J = 2.02$ Hz, 1H), 6.23 (d, $J = 9.1$ Hz, 1H), 4.61 (d, 2H).

N,N'-(1H-indole-4,7-diyl)bis(4-methoxybenzenesulfonamide) (27)—This previously unreported compound was synthesized in a manner similar to a published procedure.[40] Pd/C (10%, 0.1 g) was added to a suspension of *N*-benzyl-7-nitro-1*H*-indol-4-amine (1.0 g, 3.7 mmol) in HCl/EtOH (1.25 M, 15 mL) and EtOH (10 mL), and the reaction mixture was hydrogenated using a Parr shaker apparatus (35 psi H$_2$) at room temperature for 24 h. On completion the reaction was filtered over Celite®, and the filter bed was washed with EtOH (20 mL). The combined organic portions were evaporated and dried to yield 0.83 g (quant. yield) of **26** as a brown solid, of which 0.3 g (0.8 mmol) was added to a solution of *p*-methoxybenzenesulfonyl chloride (0.4 g, 1.9 mmol) in pyridine (4 mL). The mixture was allowed to stir overnight at room temperature. On completion, the reaction mixture was diluted with EtOAc (50 mL) and washed with H$_2$O (2 × 100 mL), HCl (2N, 50 mL) and brine (30 mL); dried (Na$_2$SO$_4$); and evaporated to yield a crude product which, upon washing with Et$_2$O (100 mL), yielded 0.4 g (60% yield) of **27** as a buff-colored solid. ^{1}H NMR (400 MHz, DMSO-d_6, δ): 10.69 (s, 1H), 9.79 (s, 1H), 9.61 (s, 1H), 7.59 (d, $J = 8.3$ Hz, 4H), 6.96 (dd, $J = 8.4, 14.5$ Hz, 4H), 6.66 (d, $J = 7.8$ Hz, 1H), 6.45–6.61 (m, 2H), 3.78 (s, 3H), 3.75 (s, 3H); ^{13}C NMR (100 MHz, DMSO-d_6 δ): 162.4, 162.2, 131.9, 131.2, 130.9, 129.1, 128.9, 126.8, 125.1, 123.7, 118.9, 115.1, 114.2, 114.1, 112.1, 100.1, 55.6, 55.6; HRMS-ESI (+) (*m/z*): [M+H]$^+$ calcd for C$_{22}$H$_{22}$N$_3$O$_6$S$_2$, 488.0905; found, 488.0937.

2,2'-((1H-indole-4,7-diyl)bis(((4-methoxyphenyl)sulfonyl)azanediyl))diacetic acid (29)—This previously unreported compound was synthesized in a manner similar to a published procedure.[28] Potassium carbonate (0.08 g, 0.6 mmol) and *tert*-butylbromoacetate (0.08 g, 0.4 mmol) were added to a solution of **27** (0.1 g, 0.2 mmol) in anhydrous DMF (2 mL), and the reaction was stirred for 6 h at room temperature. On completion the reaction was quenched with H$_2$O (25 mL) and extracted with EtOAc (2 × 40 mL). The combined organic portion was washed with H$_2$O (2 × 100 mL) and brine (50 mL), dried (Na$_2$SO$_4$), and evaporated to yield a crude brown solid which was further washed with hexanes (30 mL) to yield 0.12 g (82% yield) of the *tert*-butyl ester **28**. Trifluoroacetic acid (0.5 mL) was added to a solution of the *tert*-butyl ester (0.06 g) in anhydrous CH$_2$Cl$_2$ (4 mL), and the reaction was stirred at room temperature for 5 h. On completion the solvent was evaporated and the crude residue (0.04 g) was purified using preparative HPLC (C18, 50% MeCN with 0.1% formic acid, retention time = 8.8 min, run length = 32 min, 4 mL/min) to yield 10 mg of **29** as a buff-colored solid. ^{1}H NMR (400 MHz, DMSO-d_6, δ): 12.85 (br. s, 1H), 11.19 (br. s, 1H), 7.47–7.68 (m, 4H), 7.25 (br s, 1H), 7.00 (d, $J = 8.8$ Hz, 2H), 7.03 (d, $J = 8.8$ Hz, 2H), 6.64 (d, $J = 8.1$ Hz, 1H), 6.55 (d, $J = 7.8$ Hz, 1H), 6.11 (s, 1H), 4.34 (s, 4H), 3.84 (s, 3H), 3.82 (s, 3H); ^{13}C NMR (100 MHz, DMSO-d_6 δ): 162.7, 162.6, 135.0, 131.4, 130.7, 129.9, 129.6, 128.0, 126.6, 124.2, 120.2, 114.2, 114.1, 100.1, 55.7, 55.7; HRMS-ESI (+) (*m/z*): [M+Na]$^+$ calcd for C$_{26}$H$_{25}$N$_3$O$_{10}$S$_2$, 626.0879; found, 626.0867.

1,4-diaminophthalazine (31)—This previously reported compound was synthesized according to a published procedure.[57] A solution of phthalonitrile (2.6 g, 20 mmol) and hydrazine hydrate (55%, 16.4 mL), in MeOH (100 mL) was stirred overnight at room temperature and refluxed for 2 h. On completion, the organic solvent was partially evaporated until a precipitate formed, which was dissolved using hot MeOH to yield 2 g (65% yield) of **31** as yellow-colored needles. ^{1}H NMR (400 MHz, DMSO-d_6, δ) 8.13–8.08 (m, 2H), 7.83–7.77 (m, 2H), 5.94 (br. s, 4H).

N,N'-(phthalazine-1,4-diyl)bis(4-methoxybenzenesulfonamide) (32)—This previously unreported compound was synthesized in a manner similar to a published procedure.[51] A solution of 1,4-diaminophthalazine **31** (0.3 g, 1.9 mmol) and *p*-methoxybenzenesulfonyl chloride (0.85 g, 4.1 mmol) in pyridine (3 mL) and 1,4-dioxane (10 mL) was allowed to stir overnight at reflux. On completion, the reaction mixture was quenched with H_2O (100 mL), and the precipitate was collected by filtration. The collected solid was further washed with Et_2O (3 × 30 mL), and the crude product was recrystallized with HCl in EtOH (1.2 M) to obtain **32** (0.3 g, 31% yield) as a buff-colored solid. ^{1}H NMR (400 MHz, DMSO-d_6, δ) 11.50 (br. s, 1H), 8.14–8.28 (m, 2H), 7.82 (d, $J = 8.8$ Hz, 6H), 6.96 (d, $J = 8.6$ Hz, 4H). 3.78 (s, 3H); ^{13}C NMR (100 MHz, DMSO-d_6, δ) 163.0, 148.7, 143.2, 133.0, 131.4, 131.2, 129.4, 127.4, 124.8, 124.3, 116.1, 114.7, 56.1; HRMS-ESI (+) (*m/z*): [M+H]+ calcd for $C_{22}H_{20}N_4O_6S_2$, 501.0858; found, 501.0908.

Ethyl N-(4-((4-methoxyphenyl)sulfonamido)phthalazin-1-yl)-N-((4-methoxyphenyl)sulfonyl)glycinate (33)—This previously unreported compound was synthesized in a manner similar to a published procedure.[1] Lithium *tert*-butoxide (0.06 g, 0.8 mmol) and ethyl bromoacetate (0.1 g, 0.6 mmol) were added to a solution of **32** (0.05g, 0.1 mmol) in anhydrous DMF (3 mL), and the reaction was stirred for 24 h at room temperature. On completion the reaction was quenched with 2N HCl (25 mL), and the buff-colored solid was collected by filtration to yield 0.06 g (quant. yield) of a brown solid. 30 mg of this crude material was subjected to purification using preparative HPLC to yield 10 mg of **33** as a white solid. ^{1}H NMR (400 MHz, CD_3CN, δ) 8.45–8.55 (m, 1H), 8.41 (dd, $J = 8.2, 0.6$ Hz, 1H), 7.99–8.13 (m, 1H), 7.89–7.99 (m, 3H), 7.68–7.83 (m, 2H), 7.09–7.15 (m, 2H), 7.02–7.09 (m, 2H), 4.03 (q, $J = 7.1$ Hz, 2H), 3.94 (s, 3H), 3.86 (s, 3H), 1.06 (t, $J = 7.1$ Hz, 3H); ^{13}C NMR (100 MHz, CD_3CN, δ) 167.6, 164.1, 162.8, 134.4, 134.4, 133.4, 130.9, 129.3, 129.2, 128.2, 127.5, 125.6, 114.5, 114.1, 61.4, 55.7, 55.4, 51.7, 13.2; HRMS-ESI (+) (*m/z*): [M+H]+ calcd for $C_{26}H_{26}N_4O_8S_2$, 587.1226; found, 587.1220.

N-(4-((4-methoxyphenyl)sulfonamido)phthalazin-1-yl)-N-((4-methoxyphenyl)sulfonyl)glycine (34)—This previously unreported compound was synthesized in a manner similar to a published procedure.[1] 35 mg of ester **33** was suspended in NaOH (10%, 2 mL) and MeOH (10 mL) and allowed to reflux for 3 h. On completion the reaction mixture was cooled, and the organic solvent was evaporated, diluted with H_2O (10 mL), and washed with Et_2O (20 mL). The aqueous portion was acidified with HCl (2N, to pH 2), and the precipitate was collected by filtration to yield 18 mg of crude product, which was purified using preparative HPLC to yield 10 mg of **34** as a white solid. ^{1}H NMR (400 MHz, CD_3CN, δ) 8.49 (d, $J = 7.8$ Hz, 1H), 8.38 (d, $J = 8.1$ Hz, 1H), 7.98–8.08 (m, 1H), 7.94

(d, $J = 9.1$ Hz, 2H), 7.85–7.92 (m, 1H), 7.72 (d, $J = 9.1$ Hz, 2H), 7.00–7.16 (m, 4H), 4.24 (br s, 2H), 3.92 (s, 3H), 3.86 (s, 3H); ^{13}C NMR (100 MHz, CD$_3$CN, δ) 164.1, 163.0, 146.6, 134.4, 133.4, 131.0, 129.7, 128.4, 127.6, 125.6, 117.5, 114.6, 114.3, 55.8, 55.6; HRMS-ESI (+) (*m/z*): [M+H]$^+$ calcd for C$_{24}$H$_{22}$N$_4$O$_8$S$_2$, 559.0913; found, 559.0915.

Methyl ((4-methoxyphenyl)sulfonyl)glycinate (36a)—This previously reported compound was synthesized according to a published procedure.[58] A solution of glycine methyl ester hydrochloride (1.0 g, 7.9 mmol) and *p*-methoxybenzenesulfonyl chloride (1.8 g, 8.7 mmol) in pyridine (7 mL) was allowed stir at room temperature for 24 h. On completion, the reaction mixture was quenched with HCl (2N, 30 mL) and ice. The white precipitate was collected by filtration and washed with H$_2$O (2 × 50 mL) to yield the crude product, which upon recrystallization from *i*-PrOH yielded 1.2 g (58% yield) of **36a** as white needles. ^{1}H NMR (400 MHz, DMSO-*d*$_6$, δ) 8.02 (t, $J = 6.2$ Hz, 1H), 7.67–7.77 (m, $J = 8.6$ Hz, 2H), 7.05–7.17 (m, $J = 8.8$ Hz, 2H), 3.84 (s, 3H), 3.65 (d, $J = 6.1$ Hz, 2H), 3.53 (s, 3H).

***Tert*-butyl ((4-methoxyphenyl)sulfonyl)glycinate (36b)**—This previously reported compound was synthesized according to a published procedure.[58] A solution of glycine *tert*-butyl ester hydrochloride (0.31 g, 1.8 mmol) and *p*-methoxybenzenesulfonyl chloride (0.4 g, 1.9 mmol) in pyridine (5 mL) was allowed to stir at room temperature for 4 h. On completion, the reaction mixture was quenched with HCl (2N, 30 mL) and ice. The yellow-colored precipitate was collected by filtration and washed with H$_2$O (2 × 50 mL) to yield 0.3 g (54% yield) of **36b** as yellow-colored solid. ^{1}H NMR (400 MHz, DMSO-*d*$_6$, δ) 7.73–7.86 (m, 2H), 6.91–7.05 (m, 2H), 3.87 (s, 3H), 3.66 (d, 2H), 1.36 (s, 9H).

2,2'-((1,2-phenylenebis(methylene))bis(((4-methoxyphenyl)sulfonyl)azanediyl))diacetic acid (38)—This previously unreported compound was synthesized in a manner similar to a published procedure.[1] Potassium carbonate (0.16 g, 1.14 mmol) and methyl ((4-methoxyphenyl)sulfonyl)glycinate **36a** (0.19 g, 0.76 mmol) were added to a solution of α,α'-dibromoxylene (0.1 g, 0.38 mmol) in anhydrous DMF (2 mL), and the reaction was stirred overnight at room temperature. On completion the reaction was quenched with H$_2$O (25 mL), and the solid was collected by filtration and recrystallized with MeOH to yield 0.17 g (70% yield) of methyl ester, of which 0.1 g was suspended in NaOH (10%, 2 mL) and MeOH (10 mL) and allowed to reflux for 4 h. On completion the reaction mixture was cooled, and the organic portion was evaporated and diluted with H$_2$O (10 mL). The solid was removed by filtration, and the filtrate was acidified with HCl (2N, to pH 2). The white-colored precipitate was collected by filtration. The crude solid was washed with Et$_2$O (2 × 20 mL) and dried to yield 0.07 g (74% yield) of **38** as a white-colored solid. ^{1}H NMR (400 MHz, DMSO-*d*$_6$, δ) 12.60 (br. s, 2H), 7.76 (d, $J = 8.6$ Hz, 4H), 7.26–7.31 (m, 2H), 7.20–7.26 (m, 2H), 7.09 (d, $J = 8.8$ Hz, 4H), 4.44 (s, 4H), 3.85 (s, 6H); ^{13}C NMR (100 MHz, DMSO-*d*$_6$, δ) 170.3, 163.0, 134.8, 130.9, 129.8, 129.1, 128.0, 114.8, 56.1, 49.5, 48.7; HRMS-ESI (+) (*m/z*): [M+Na]$^+$ calcd for C$_{26}$H$_{28}$N$_2$O$_{10}$S$_2$, 615.1083; found, 615.1068.

2,2'-(phthaloylbis(((4-methoxyphenyl)sulfonyl)azanediyl))diacetate (40)—This previously unreported compound was synthesized in a manner similar to a published

procedure.[59] *tert*-Butyl ((4-methoxyphenyl)sulfonyl)glycinate **36b** (0.15 g, 0.5 mmol) was added to a solution of phthaloyl chloride (0.05 g, 0.3 mmol) in pyridine (4 mL), and the reaction was stirred overnight at room temperature. On completion the reaction was quenched with H_2O (25 mL) and extracted with EtOAc (2 × 40 mL). The combined organic portions were washed with HCl (2N, 2 × 50 mL), H_2O (2 × 100 mL), and brine (50 mL); dried (Na_2SO_4); and evaporated to yield a brown oil as crude product which was further purified by column chromatography (silica gel; Hexanes/EtOAc; 100:10 to 100:45) to afford 0.1 g (55% yield) of the *tert*-butyl ester of **39**. Trifluoroacetic acid (0.5 mL) was added to a solution of the *tert*-butyl ester (0.05 g) in anhydrous CH_2Cl_2 (4 mL), and the reaction was stirred at room temperature overnight. On completion the solvent was evaporated, and the crude residue was recrystallized from *i*-PrOH to yield 0.02 g (50% yield) **40** as a white solid. ^{1}H NMR (400 MHz, DMSO-d_6, δ) 7.87 (d, $J = 8.3$ Hz, 4H), 7.58 (br s, 2H), 7.44 (br s, 2H), 7.11 (d, $J = 8.5$ Hz, 4H), 4.18 (s, 4H), 3.86 (s, 6H); ^{13}C NMR (100 MHz, DMSO-d_6 δ) 170.7, 164.0, 162.5, 136.7, 136.3, 130.5, 129.1, 125.8, 115.1, 114.6, 56.1; HRMS-ESI (+) (*m/z*): [M+Na]+ calcd for $C_{26}H_{24}N_2O_{12}S_2$, 643.0668; found, 643.0634.

(*E/Z*)-2,2'-(but-2-ene-1,4-diyl)bis(((4-methoxyphenyl)sulfonyl)azanediyl))diacetate (42)

This previously unreported compound was synthesized in a manner similar to a published procedure.[1] Potassium carbonate (0.19 g, 1.4 mmol) and methyl ((4-methoxyphenyl)sulfonyl)glycinate **36a** (0.24 g, 0.94 mmol) were added to a solution of 1,4-dibromobutene (0.1 g, 0.47 mmol) in anhydrous DMF (2 mL), and the reaction was stirred overnight at room temperature. On completion the reaction was quenched with H_2O (25 mL), and the solid was collected by filtration and recrystallized with acetone/*i*-PrOH to yield 0.22 g (80% yield) of methyl ester of which 0.15 g was suspended in NaOH (10%, 2 mL) and MeOH (10 mL) and allowed to reflux for 4 h. On completion the reaction mixture was cooled, the organic portion was evaporated and diluted with H_2O (10 mL). The solid was removed by filtration, and the filtrate was acidified with HCl (2N, to pH 2). The white-colored precipitate was collected by filtration. The crude solid was washed with Et_2O (2 × 20 mL) and dried to yield 0.1 g (70% yield) of **42** as a white-colored solid. 12.68 (br. s, 2H), 7.72 (d, $J = 8.8$ Hz, 4H), 7.09 (d, $J = 8.8$ Hz, 4H), 5.40 (br. s, 2H), 3.84 (s, 7H), 3.79 (s, 4H), 3.73 (br. s, 4H); ^{13}C NMR (100 MHz, DMSO-d_6, δ) 170.5, 162.9, 131.6, 129.6, 129.0, 114.8, 56.1, 49.5, 47.7; HRMS-ESI (+) (*m/z*): [M+Na]+ calcd for $C_{22}H_{26}N_2O_{10}S_2$, 565.0927; found, 565.0932.

3,5-dinitro-1,1'-biphenyl

This previously unreported compound was synthesized in a manner similar to a published procedure.[60] 1-Bromo-3,5-dinitrobenzene (100 mg, 0.404 mmol), phenylboronic acid (54.2 mg, 0.444 mmol), Pd(OAc)$_2$ (5%, 4.9 mg) and potassium phosphate (86.0 mg, 0.405 mmol) were added to 1 mL of H_2O and allowed to reflux overnight. On completion, the reaction mixture was cooled, quenched with HCl (1N, 2 × 10mL) and extracted using ethyl acetate (10 mL) and brine (10 mL) and H_2O (2 × 10 mL), dried over Na_2SO_4, and evaporated to yield 0.176 g of a yellow-white solid. ^{1}H NMR (400 MHz, CDCl$_3$, δ) 9.04 (s, 1H), 8.80 (s, 2H), 7.74–7.69 (d, $J = 6.88$ Hz, 2H), 7.62–7.52 (m, 3H).

1,1'-biphenyl-3,5-diamine (44)—Dihydrate tin (II) chloride (0.87 g, 3.8 mmol) was added to 3,5-dinitro-1,1'-biphenyl (67 mg, 0.27 mmol) in methanol (3.9 mL) under argon and allowed to reflux for 1 hour. The reaction was quenched with excess saturated $NaHCO_3$; extracted using ethyl acetate (10 mL), brine (10 mL), and H_2O (2 × 10 mL); dried over Na_2SO_4; and evaporated to yield (0.050 g, 98.7%) of a red-brown oil. ^{1}H NMR (400 MHz, $CDCl_3$, δ) 7.60–7.53 (d, $J = 7.48$ Hz, 2H) 7.45–7.30 (m, 3H), 6.41–6.34 (s, 2H), 6.07 (s, 1H), 3.69 (s, 1H).

3*N,N'*-(1,1'-biphenyl]-3,5-diyl)bis(4-methoxybenzenesulfonamide) (45)—The biphenyl **44** (80.0 mg, 0.43 mmol) was added to 4-methoxybenzenesulfonylchloride (396 mg, 1.92 mmol) in pyridine (0.75 mL) and THF (0.5 mL) and refluxed under argon for 24 hours. The reaction was quenched with HCl (1N, 2 × 10mL); extracted using ethyl acetate (10 mL), brine (10 mL) and H_2O (2 × 10 mL); dried over Na_2SO_4; and taken to the next step. ^{1}H NMR (400 MHz, $CDCl_3$, δ) 7.76–7.71 (d, $J = 8.72$ Hz, 4H), 7.44–7.35 (m, 5H), 6.99–6.90 (m, 7H), 6.49 (s, 2H), 3.86 (s, 6H).

Diethyl 2,2'-(1,1'-biphenyl]-3,5-diylbis(((4-methoxyphenyl)sulfonyl)azanediyl)diacetate—Ethyl-2-bromoacetate (83 μL, 0.75 mmol) and the previously formed sulfonamide **45** were added to potassium carbonate (0.130 g, 0.93 mmol) and DMF (2 mL) and stirred at room temperature for 2 hours. The reaction was extracted using ethyl acetate (10 mL), brine (10 mL), and H_2O (2 × 10mL); dried over Na_2SO_4; evaporated; and taken to the next step. ^{1}H NMR (400 MHz, $CDCl_3$, δ) 7.66–7.62 (d, $J = 7.68$ Hz, 2H), 7.45–7.36 (m, 5H), 7.05–7.01 (m, 1H), 6.99–6.95 (d, $J = 9.1$ Hz, 2H), 4.35 (s, 2H), 4.20–4.13 (q, 4H), 3.89 (s, 4H), 2.07 (s, 1H), 1.56 (s, 6H), 1.31–1.21 (t, 6 H).

2,2'-(1,1'-biphenyl]-3,5-diylbis(((4-methoxyphenyl)sulfonyl)azanediyl) diacetic acid (46)—NaOH (15%) and methanol (2.4 mL) were added to the previously formed ester and allowed to reflux for 1 hour. On completion, the reaction mixture was cooled; quenched with HCl (1N, 20 mL); extracted using ethyl acetate (10 mL), brine (10 mL), and H_2O (2 × 10mL); dried over Na_2SO_4; and purified using preparative HPLC (C18, 30–95% MeCN with 0.1% formic acid) to yield a white powder (0.024 g, 51%). ^{1}H NMR (400 MHz, CD_3CN, δ) 7.64–7.57 (d, 4H), 7.50–7.37 (m, 5H) 7.37–7.32 (s, 2H), 7.05–7.00 (d, 4 H) 4.39–4.33 (s, 4H), 3.91–3.84 (s, 6H); ^{13}C NMR (100 MHz, CD_3CN, δ): 163.4, 142.2, 141.2, 138.8, 129.9, 129.0, 128.2, 126.8, 126.0, 125.8, 114.3, 55.6, 52.0; HRMS-ESI (−) (*m/z*): [M-H]$^-$ calcd for $C_{30}H_{28}N_2O_{10}S_2$, 639.1191, found 639.1149

Kelch domain expression and purification: KEAP1 Kelch domain was expressed and purified as previously described [1]

Fluorescence anisotropy assays: Fluorescence anisotropy assays were performed as previously described.[1] Briefly, small molecules ability to inhibit the KEAP1-NRF2 interaction were assayed using the Kelch domain of KEAP1 and a fluorescein-labeled 9-mer peptide containing the ETGE motif of the Neh2 domain of NRF2 [41]. The experiments were performed in triplicate and sigmoidal concentration-response curves were fitted to the data using Graphpad Prism 6.1 software

Surface Plasmon Resonance Assay: Surface Plasmon Resonance assays were performed as previously described.[1] Briefly, the Kelch domain of KEAP1 was immobilized on a CM5 sensor chip. Increasing concentrations of compound solutions were applied to the protein-bound chip, and response units were measured. The experiments were conducted in triplicate with a technical repeat. Approximately 40% of captured KEAP1 was active based on the comparison between calculated RU_{max} and achieved RU_{max}:

$$Analyte\ binding\ capacity\ \left(RU_{max}\right) = \frac{analyte\ MW}{ligand\ MW}\ x\ immobilization\ level\ \left(RU\right)$$

1-site binding saturation curves were fitted to the data using GraphPad Prism 6.1.

Gene expression analysis: Spontaneously immortalized human keratinocytes (HaCaT cell line, kindly provided by Dr. Luisa DiPietro, University of Illinois) were grown in Dubecco's modified Eagle's medium (DMEM) with 10% fetal bovine serum and 1% antibiotics. Cells at 70–80% confluence were treated with compounds as indicated for 6 h or 24 h in the presence of complete medium. Cells were lysed in a 20 mM Tris (pH 7.5) buffer containing 150 mM NaCl, 1 mM EDTA, 1 mM EGTA, 1% Triton X-100, 2.5 mM sodium pyrophosphate, 1 mM Na_3VO_4, 5 mM β-glycerophosphate, and 1 μg/mL leupeptin. Equal amount of protein (~40 μg) was separated on a 10% SDS-PAGE, blotted on the membrane, and probed with anti-NRF2 (sc-13032, Santa Cruz Biotech, Santa Cruz, CA), anti-NQO1 (A1518, Neo Scientific, Cambridge, MA) or anti-GCLM (14241–1-AP, Proteintech, Rosemont, IL) antibodies. Membranes were stripped and probed with anti-GAPDH antibodies (SC-25778, Santa Cruz Biotech, Santa Cruz, CA). The blots were developed using HyGlo-Chemi antibody detection kit (Denville Scientific Inc, Metuchen, NJ) and images were visualized on ChemiDoc (Biorad). Band intensities were quantified using ImageJ software with GAPDH intensity as a reference. The values of vehicle treated samples were considered as one arbitrary unit.

Mini-Ames Assay: A Mini-Ames Assay was used to evaluate the compounds **17** and **6a**, for their ability to induce reverse mutations at the histidine locus of strains of *Salmonella typhimurium* (TA98, TA100, TA1535, TA1537) and *Escherichia coli* (WP2 uvrA (pKM101)) in the presence and absence of exogenous metabolic activation (Aroclor 1254 induced rat liver S9). **17** and **6a** were soluble in DMSO up to 50 mg/mL; therefore DMSO was chosen as the solvent. The assay was conducted in the presence or absence of the S9 mix along with concurrent negative/solvent control and positive controls. Dose levels tested in the Mini-Ames assay were 1.5, 4, 10, 25, 64, 160, 400 and 1000 μg/well. Compound dilutions were prepared immediately prior to use.

A top agar consisting of 0.6% (w/v) agar and 0.5% (w/v) NaCl was melted. 10 mL of 0.5 mM L-histidine/biotin solution or 5 mL of 0.5 mM Tryptophan solution was added to the melted top agar per 100 mL top agar. This solution was aliquoted at 1.6 mL per tube and held at approximately 45 °C. 80 μL of the compound solution, 400 μL of S9 mix (for S9-activated) or phosphate buffered saline (for non-activated) and 80 μL of the bacterial culture were added to the 1.6 mL of top agar. After mixing the top agar mix, every 540 μL of the resulting mix was added into one well of the 6-well plates (34.8-mm dishes) containing

solidified approximately 5 mL of minimal glucose agar media (1.5% agar, 2% glucose, in Vogel-Bonner medium E). Each treatment was plated in triplicate (three wells) except vehicle control which was plated in sextuple. As soon as the soft agar solidified, the 6-well plates were incubated at 37 ± 2 °C for 48 to 72 hours. Plates were counted immediately following the incubation period.

The number of revertant colonies in each well was counted manually and recorded. Pinpoint colonies appearing on a well in conjunction with an absence of background lawn were not revertants and were not scored (Mortelmans and Zeiger, 2000).

The condition of the bacterial background lawn was evaluated for evidence of cytotoxicity. Evidence of cytotoxicity was scored relative to the negative control plate and recorded along with the revertant count for that plate. Cytotoxicity was evaluated as a decrease in the number of revertant colonies per well and/or a thinning or disappearance of the bacterial background lawn. Precipitation was evaluated after the incubation period by visual examination without magnification. Precipitation could be confirmed microscopically.

Kinetic Solubility Studies: A variation of a previously reported method was employed to determine the compounds' solubility in buffer at pH 7.4.[61]Briefly, 10 mM DMSO stock solutions of compounds were diluted to 400 μM in buffer (200 mM HEPES, 150 mM NaCl, pH 7.4). The mixture was stirred for 1 hr, filtered, and then injected onto a Shimadzu LC-20AB HPLC system (Solvent system: gradient from 15% MeCN/85% H_2O to 95% MeCN/5% H_2O (+0.1% formic acid) over 13 minutes; Column: Shimadzu C18, 50 μm, 50 × 4.6 mm; (UV, 254 nm). A 10 mM stock solution was prepared by completely dissolving test compound in DMSO. This solution was diluted to six known concentration solutions (1200 μM, 400 μM, 120 μM, 40 μM, 12 μM, and 4 μM) in MeCN. Each solution was analyzed by HPLC, and a calibration curve was plotted using the peak areas from the standard concentrations. The equilibrium solubility of test compounds was determined by quantifying the concentration of test solutions against the calibration curve. (SI Figure S10). Experiments were run in triplicate and results were tabulated and reported as mean ± standard deviation (Table 2).

2-D NMR Studies: Standard pulse programs found in the Bruker TopSpin™ 3.x software library were applied for detecting direct (HSQC) and long-range heteronuclear correlations (HMBC), as well as through-space correlations (2D NOESY and selective 1D NOESY). Phase sensitive HSQC experiment was acquired with the heteronuclear one bond coupling constant of 145 Hz, 32 scans per increment, relaxation delay of 1.5 s, 2048 and 128 data points in direct and indirect dimension, respectively. The HMBC experiments were acquired with the heteronuclear long range coupling constants of 2 and 8 Hz, with the number of data points set to 2048 × 512 or 2048 × 384, respectively. Carbon spectra obtained with DEPTQ135 experiment served as an external reference. For the 2D NOESY using purge pulses and gradients, the number of data points were set to 2048 × 192, with the relaxation time of 2 s and mixing time of 0.8 s. The data were processed using square sine-bell weighting functions in both dimensions. One dimensional gradient-selective NOESY experiments were performed with the Gaussian pulse of 2 ms and the relaxation mixing time of 0.6 s.

Metabolism Studies:

Materials.: LC-MS grade acetonitrile (MeCN), methanol (MeOH) and formic acid, biology grade DMSO were purchased from Fisher Scientific (Pittsburgh, PA). LC-MS grade water was generated using a Barnstead™ Nanopure Diamond water system (Thermo Scientific, Pittsburgh, PA). All other reagents, if not specified, were purchased from Sigma Aldrich (Saint Louis, MO). Pooled human liver microsomes and mouse liver microsomes were purchased from Sekisui XenoTech (Kansas City, KS).

Preparation of standard.: The initial stock solutions of test compounds were prepared in DMSO at 10 mM, and then diluted with MeOH to 200 μM before use. All stock solutions were stored at −20 °C. Liver microsomes were aliquoted upon arrival and stored at −80 °C.

Liquid chromatographic and mass spectrometric conditions.: Samples were analyzed on a Shimadzu 8040 triple-quadrupole mass spectrometer (Shimadzu, Addison, IL) equipped with electrospray ion source and Shimadzu Nexera XR UHPLC system. Mobile phase A contained water with 0.025% (v/v) FA, mobile phase B consisting of MeCN with 0.1% (v/v) FA. 5 μL of sample was injected. Study compounds were eluted on a Kinetex C18 column (3.0 × 50 mm, 2.6 μm; Phenomenex, Torrance, CA) at 500 μL/min using a gradient program: mobile phase B started and maintained at 15% for 1 min, then increased to 95% in 4 min.

Mass spectrometric analysis was performed in positive mode for all study compounds except **6a** using multiple reaction monitoring (MRM). Nebulizing gas flow and drying gas flow were set to 2 L/min and 15 L/min. DL temperature, heat block temperature and ion spray voltage were maintained at 300 °C, 450 °C and 4500 V, respectively. The precursor ion and product ion of each compound and corresponding Q1 Pre Bias, collision energy (CE) and Q3 Pre Bias are listed in Table 3.

Microsomal stability.: The microsomal stability of study compounds was assessed using human liver microsomes and mouse liver microsomes individually. Briefly, pooled liver microsomes (0.5 mg/mL) were pre-incubated with 1 μM of the study compound in potassium phosphate buffer (100 mM, pH 7.4) at 37 °C for 5 min. The reaction was initiated by adding freshly prepared NADPH (1.5 mM) and quenched by adding equal volume of cold MeCN at 20 min after incubation. Samples were kept at −20 °C for 10 min, followed by centrifugation at 14000 rpm at 4 °C for 15 min. The supernatant was extracted and diluted two times with a mixture of MeCN : water (50:50, v/v). The resulting solution was analyzed by LC-MS. Peak area of each target compound was used for quantitation. Each compound was also incubated in buffer only, and without NADPH. The metabolic stability of the study compound was determined by the percentage of compound remaining after the incubation.

Supplementary Material

Refer to Web version on PubMed Central for supplementary material.

Acknowledgments:

Abbreviations Used:

ARE	antioxidant response element
BTB	Tramtrack and Bric-à-Brac
CUL3	cullin 3
DMEM	Dulbecco's Modified Eagle's Medium
DMF	*N,N*-dimethylformamide
DMSO	dimethyl sulfoxide
EtOAc	ethyl acetate
GAPDH	Glyceraldehyde 3-phosphate dehydrogenase
GCLM	Glutamate-Cysteine Ligase Modifier
HEPES	4-(2-hydroxyethyl)-1-piperazineethanesulfonic acid
HMBC	heteronuclear multiple bond correlation
HMOX1	heme oxygenase 1
HPLC	high-performance liquid chromatography
HRMS	high resolution mass spectrometry
HSQC	heteronuclear single quantum correlation
IVR	intervening region
KEAP1	kelch-like ECH associated protein 1
LC-MS	liquid chromatography mass spectrometry
NADPH	nicotinamide adenine dinucleotide phosphate
NOESY	Nuclear Overhauser Effect Spectroscopy
NQO1	NAD(P)H quinone dehydrogenase 1
NRF2	nuclear factor (erythroid-derived 2)-like 2
TFA	trifluoroacetic acid
THF	tetrahydrofuran
UHPLC	ultra-high performance liquid chromatography

References

1. Jain AD; Potteti H; Richardson BG; Kingsley L; Luciano JP; Ryuzoji AF; Lee H; Krunic A; Mesecar AD; Reddy SP; Moore TW Probing the structural requirements of non-electrophilic naphthalene-based Nrf2 activators. Eur. J. Med. Chem 2015, 103, 252–268. [PubMed: 26363505]

2. Itoh K; Chiba T; Takahashi S; Ishii T; Igarashi K; Katoh Y; Oyake T; Hayashi N; Satoh K; Hatayama I; Yamamoto M; Nabeshima Y An Nrf2/small Maf heterodimer mediates the induction of phase II detoxifying enzyme genes through antioxidant response elements. Biochem. Biophys. Res. Commun 1997, 236, 313–322. [PubMed: 9240432]

3. Itoh K; Wakabayashi N; Katoh Y; Ishii T; Igarashi K; Engel JD; Yamamoto M Keap1 represses nuclear activation of antioxidant responsive elements by Nrf2 through binding to the amino-terminal Neh2 domain. Genes Dev. 1999, 13, 76–86. [PubMed: 9887101]

4. Cullinan SB; Gordan JD; Jin J; Harper JW; Diehl JA The Keap1-BTB protein is an adaptor that bridges Nrf2 to a Cul3-based E3 ligase: oxidative stress sensing by a Cul3-Keap1 ligase. Mol. Cell. Biol 2004, 24, 8477–8486. [PubMed: 15367669]

5. Furukawa M; Xiong Y BTB protein Keap1 targets antioxidant transcription factor Nrf2 for ubiquitination by the Cullin 3-Roc1 ligase. Mol. Cell. Biol 2005, 25, 162–171. [PubMed: 15601839]

6. Lo SC; Li X; Henzl MT; Beamer LJ; Hannink M Structure of the Keap1:Nrf2 interface provides mechanistic insight into Nrf2 signaling. EMBO J. 2006, 25, 3605–3617. [PubMed: 16888629]

7. McMahon M; Thomas N; Itoh K; Yamamoto M; Hayes JD Dimerization of substrate adaptors can facilitate cullin-mediated ubiquitylation of proteins by a "tethering" mechanism: a two-site interaction model for the Nrf2-Keap1 complex. J. Biol. Chem 2006, 281, 24756–24768. [PubMed: 16790436]

8. Tong KI; Katoh Y; Kusunoki H; Itoh K; Tanaka T; Yamamoto M Keap1 recruits Neh2 through binding to ETGE and DLG motifs: characterization of the two-site molecular recognition model. Mol. Cell. Biol 2006, 26, 2887–2900. [PubMed: 16581765]

9. Tong KI; Kobayashi A; Katsuoka F; Yamamoto M Two-site substrate recognition model for the Keap1-Nrf2 system: a hinge and latch mechanism. Biol. Chem 2006, 387, 1311–1320. [PubMed: 17081101]

10. Ohtsubo T; Kamada S; Mikami T; Murakami H; Tsujimoto Y Identification of NRF2, a member of the NF-E2 family of transcription factors, as a substrate for caspase-3(-like) proteases. Cell Death Differ. 1999, 6, 865–872. [PubMed: 10510468]

11. Hayes JD; Chanas SA; Henderson CJ; McMahon M; Sun C; Moffat GJ; Wolf CR; Yamamoto M The Nrf2 transcription factor contributes both to the basal expression of glutathione S-transferases in mouse liver and to their induction by the chemopreventive synthetic antioxidants, butylated hydroxyanisole and ethoxyquin. Biochem. Soc. Trans 2000, 28, 33–41. [PubMed: 10816095]

12. Dinkova-Kostova AT; Holtzclaw WD; Cole RN; Itoh K; Wakabayashi N; Katoh Y; Yamamoto M; Talalay P Direct evidence that sulfhydryl groups of Keap1 are the sensors regulating induction of phase 2 enzymes that protect against carcinogens and oxidants. Proc. Natl. Acad. Sci. U S A 2002, 99, 11908–11913. [PubMed: 12193649]

13. Kwak MK; Wakabayashi N; Greenlaw JL; Yamamoto M; Kensler TW Antioxidants enhance mammalian proteasome expression through the Keap1-Nrf2 signaling pathway. Mol. Cell. Biol 2003, 23, 8786–8794. [PubMed: 14612418]

14. McMahon M; Itoh K; Yamamoto M; Hayes JD Keap1-dependent proteasomal degradation of transcription factor Nrf2 contributes to the negative regulation of antioxidant response element-driven gene expression. J. Biol. Chem 2003, 278, 21592–21600. [PubMed: 12682069]

15. Nguyen T; Sherratt PJ; Huang HC; Yang CS; Pickett CB Increased protein stability as a mechanism that enhances Nrf2-mediated transcriptional activation of the antioxidant response element. Degradation of Nrf2 by the 26 S proteasome. J. Biol. Chem 2003, 278, 4536–4541. [PubMed: 12446695]

16. Richardson BG; Jain AD; Speltz TE; Moore TW Non-electrophilic modulators of the canonical Keap1/Nrf2 pathway. Bioorg. Med. Chem. Lett 2015, 25, 2261–2268. [PubMed: 25937010]

17. Baird L; Swift S; Lleres D; Dinkova-Kostova AT Monitoring Keap1-Nrf2 interactions in single live cells. Biotechnol. Adv 2014, 32, 1133–1144. [PubMed: 24681086]

18. Crunkhorn S Deal watch: Abbott boosts investment in NRF2 activators for reducing oxidative stress. Nat. Rev. Drug. Discov 2012, 11, 96.

19. Magesh S; Chen Y; Hu L Small molecule modulators of Keap1-Nrf2-ARE pathway as potential preventive and therapeutic agents. Med. Res. Rev 2012, 32, 687–726. [PubMed: 22549716]

20. Mitsuishi Y; Motohashi H; Yamamoto M The Keap1-Nrf2 system in cancers: stress response and anabolic metabolism. Front. Oncol 2012, 2, 200. [PubMed: 23272301]

21. Yore MM; Kettenbach AN; Sporn MB; Gerber SA; Liby KT Proteomic analysis shows synthetic oleanane triterpenoid binds to mTOR. PLoS One 2011, 6, e22862. [PubMed: 21818401]

22. Clulow JA; Storck EM; Lanyon-Hogg T; Kalesh KA; Jones LH; Tate EW Competition-based, quantitative chemical proteomics in breast cancer cells identifies new target profiles for sulforaphane. Chem. Commun 2017, 53, 5182–5185.

23. Schulze-Topphoff U; Varrin-Doyer M; Pekarek K; Spencer CM; Shetty A; Sagan SA; Cree BA; Sobel RA; Wipke BT; Steinman L; Scannevin RH; Zamvil SS Dimethyl fumarate treatment induces adaptive and innate immune modulation independent of Nrf2. Proc. Natl. Acad. Sci. U S A 2016, 113, 4777–4782. [PubMed: 27078105]

24. Davies TG; Wixted WE; Coyle JE; Griffiths-Jones C; Hearn K; McMenamin R; Norton D; Rich SJ; Richardson C; Saxty G; Willems HM; Woolford AJ; Cottom JE; Kou JP; Yonchuk JG; Feldser HG; Sanchez Y; Foley JP; Bolognese BJ; Logan G; Podolin PL; Yan H; Callahan JF; Heightman TD; Kerns JK Monoacidic Inhibitors of the Kelch-like ECH-Associated Protein 1: Nuclear Factor Erythroid 2-Related Factor 2 (KEAP1:NRF2) Protein-Protein Interaction with High Cell Potency Identified by Fragment-Based Discovery. J. Med. Chem 2016, 59, 3991–4006. [PubMed: 27031670]

25. Hu L; Magesh S; Chen L; Wang L; Lewis TA; Chen Y; Khodier C; Inoyama D; Beamer LJ; Emge TJ; Shen J; Kerrigan JE; Kong AN; Dandapani S; Palmer M; Schreiber SL; Munoz B Discovery of a small-molecule inhibitor and cellular probe of Keap1-Nrf2 protein-protein interaction. Bioorg. Med. Chem. Lett 2013, 23, 3039–3043. [PubMed: 23562243]

26. London N; Raveh B; Schueler-Furman O Druggable protein–protein interactions – from hot spots to hot segments. Curr. Opin. Chem. Biol 2013, 17, 952–959. [PubMed: 24183815]

27. Marcotte D; Zeng W; Hus JC; McKenzie A; Hession C; Jin P; Bergeron C; Lugovskoy A; Enyedy I; Cuervo H; Wang D; Atmanene C; Roecklin D; Vecchi M; Vivat V; Kraemer J; Winkler D; Hong V; Chao J; Lukashev M; Silvian L Small molecules inhibit the interaction of Nrf2 and the Keap1 Kelch domain through a non-covalent mechanism. Bioorg. Med. Chem 2013, 21, 4011–4019. [PubMed: 23647822]

28. Jiang ZY; Lu MC; Xu LL; Yang TT; Xi MY; Xu XL; Guo XK; Zhang XJ; You QD; Sun HP Discovery of potent Keap1-Nrf2 protein-protein interaction inhibitor based on molecular binding determinants analysis. J. Med. Chem 2014, 57, 2736–2745. [PubMed: 24512214]

29. Jiang ZY; Xu LL; Lu MC; Pan Y; Huang HZ; Zhang XJ; Sun HP; You QD Investigation of the intermolecular recognition mechanism between the E3 ubiquitin ligase Keap1 and substrate based on multiple substrates analysis. J. Comput. Aided. Mol. Des 2014, 28, 1233–1245. [PubMed: 25301376]

30. Lu MC; Tan SJ; Ji JA; Chen ZY; Yuan ZW; You QD; Jiang ZY Polar recognition group study of Keap1-Nrf2 protein-protein interaction inhibitors. ACS Med. Chem. Lett 2016, 7, 835–840. [PubMed: 27660687]

31. Winkel AF; Engel CK; Margerie D; Kannt A; Szillat H; Glombik H; Kallus C; Ruf S; Gussregen S; Riedel J; Herling AW; von Knethen A; Weigert A; Brune B; Schmoll D Characterization of RA839, a noncovalent small molecule binder to Keap1 and selective activator of Nrf2 signaling. J. Biol. Chem 2015, 290, 28446–28455. [PubMed: 26459563]

32. Schwarz LR; Mezger M; Hesse S Effect of decreased glucuronidation and sulfation on covalent binding of naphthalene in isolated rat hepatocytes. Toxicol. 1980, 17, 119–122.

33. Buckpitt A; Boland B; Isbell M; Morin D; Shultz M; Baldwin R; Chan K; Karlsson A; Lin C; Taff A; West J; Fanucchi M; Van Winkle L; Plopper C Naphthalene-induced respiratory tract toxicity: metabolic mechanisms of toxicity. Drug Metab. Rev 2002, 34, 791–820. [PubMed: 12487150]

34. Tsuruda LS; Lame MW; Jones AD Formation of epoxide and quinone protein adducts in B6C3F1 mice treated with naphthalene, sulfate conjugate of 1,4-dihydroxynaphthalene and 1,4-naphthoquinone. Arch. Toxicol 1995, 69, 362–367. [PubMed: 7495373]

35. Buckpitt AR; Warren DL Evidence for hepatic formation, export and covalent binding of reactive naphthalene metabolites in extrahepatic tissues in vivo. J. Pharmacol. Exp. Ther 1983, 225, 8–16. [PubMed: 6834280]

36. Hsu KH; Su BH; Tu YS; Lin OA; Tseng YJ Mutagenicity in a molecule: Identification of core structural features of mutagenicity using a scaffold analysis. PLoS One 2016, 11, e0148900. [PubMed: 26863515]

37. Bulbulyan MA; Figgs LW; Zahm SH; Savitskaya T; Goldfarb A; Astashevsky S; Zaridze D Cancer incidence and mortality among beta-naphthylamine and benzidine dye workers in Moscow. Int. J. Epidemiol 1995, 24, 266–275. [PubMed: 7635585]

38. Rafferty MF No denying it: Medicinal chemistry training is in big trouble. J. Med. Chem 2016, 59, 10859–10864. [PubMed: 27668824]

39. Garst ME; Lukton D Phenyldiazenes from phenyl diazonium fluoborate and carbanions. Synth. Commun 1980, 10, 155–160.

40. Wuts PGM; Greene TW Protection for the amino group In Greene's Protective Groups in Organic Synthesis, John Wiley & Sons, Inc., Hoboken, New Jersey: 2006; pp 696–926.

41. Inoyama D; Chen Y; Huang X; Beamer LJ; Kong AN; Hu L Optimization of fluorescently labeled Nrf2 peptide probes and the development of a fluorescence polarization assay for the discovery of inhibitors of Keap1-Nrf2 interaction. J. Biomol. Screen 2012, 17, 435–447. [PubMed: 22156223]

42. Dougherty DA Cation-pi interactions in chemistry and biology: a new view of benzene, Phe, Tyr, and Trp. Science 1996, 271, 163–168. [PubMed: 8539615]

43. Dougherty DA Cation-pi interactions involving aromatic amino acids. J. Nutr 2007, 137, 1504S–1508S; discussion 1516S-1517S. [PubMed: 17513416]

44. Dougherty DA The cation-pi interaction. Acc. Chem. Res 2013, 46, 885–893. [PubMed: 23214924]

45. Pallesen JS; Tran KT; Bach A Non-covalent small-molecule Kelch-like ECH-Associated Protein 1-Nuclear Factor Erythroid 2-Related Factor 2 (Keap1-Nrf2) inhibitors and their potential for targeting central nervous system diseases. J. Med. Chem 10.1021/acs.jmedchem.8b00358. Published Online: May 11, 2018.

46. Yasuda D; Yuasa A; Obata R; Nakajima M; Takahashi K; Ohe T; Ichimura Y; Komatsu M; Yamamoto M; Imamura R; Kojima H; Okabe T; Nagano T; Mashino T Discovery of benzo[g]indoles as a novel class of non-covalent Keap1-Nrf2 protein-protein interaction inhibitor. Bioorg. Med. Chem. Lett 2017, 27, 5006–5009. [PubMed: 29037947]

47. Drwal MN; Banerjee P; Dunkel M; Wettig MR; Preissner R ProTox: a web server for the in silico prediction of rodent oral toxicity. Nucleic Acids Res. 2014, 42, W53–58. [PubMed: 24838562]

48. Maunz A; Gutlein M; Rautenberg M; Vorgrimmler D; Gebele D; Helma C Lazar: a modular predictive toxicology framework. Front. Pharmacol 2013, 4, 38. [PubMed: 23761761]

49. Lu M; Zhou HS; You QD; Jiang Z Design, synthesis, and initial evaluation of affinity-based small-molecule probes for fluorescent visualization and specific detection of Keap1. J. Med. Chem 2016, 59, 7305–7310. [PubMed: 27409246]

50. Jiang ZY; Xu LL; Lu MC; Chen ZY; Yuan ZW; Xu XL; Guo XK; Zhang XJ; Sun HP; You QD Structure-activity and structure-property relationship and exploratory in vivo evaluation of the nanomolar Keap1-Nrf2 protein-protein interaction inhibitor. J. Med. Chem 2015, 58, 6410–6421. [PubMed: 26258437]

51. Briffett NE; Hibbert F Alkaline hydrolysis of dibenzoylaminonaphthalenes in 70%(v/v) Me2SO-H2O and the effect of a neighbouring amide group. J. Chem. Soc., Perkin Trans. 2 1989, 7, 765–768.

52. Dumas JP; Joe TK; Kluender HCE; Lee W; Nagarathnam D; Sibley RN; Su N; Boyer SJ; Dixon JA Preparation of Substituted Pyridines and Pyridazines with Angiogenesis Inhibiting Activity for Pharmaceutical use as Antitumor Agents. WO2001023375A2, 2001.

53. Qin H-L; Panek JS Total synthesis of the Hsp90 inhibitor geldanamycin. Org. Lett 2008, 10, 2477–2479. [PubMed: 18489177]

54. Wrona IE; Gozman A; Taldone T; Chiosis G; Panek JS Synthesis of reblastatin, autolytimycin, and non-benzoquinone analogues: potent inhibitors of Heat Shock Protein 90. J. Org. Chem 2010, 75, 2820–2835. [PubMed: 20392070]

55. Price CC; Voong S-T 4-Nitro-1-naphthylamine. Org. Synth 1948, 28, 80–81.

56. Liu K; Yin D Efficient method for the synthesis of 2,3-unsubstituted nitro containing indoles from o-fluoronitrobenzenes. Org. Lett 2009, 11, 637–639. [PubMed: 19108672]

57. Haider N; Holzer W Product class 10: Phthalazines. Sci. Synth 2004, 16, 315–372.

58. Attolino E; Calderone V; Dragoni E; Fragai M; Richichi B; Luchinat C; Nativi C Structure-based approach to nanomolar, water soluble matrix metalloproteinases inhibitors (MMPIs). Eur. J. Med. Chem 2010, 45, 5919–5925. [PubMed: 20965620]

59. Thompson QE The diacylation of amides by acyl chloride—pyridine compounds. J. Am. Chem. Soc 1951, 73, 5841–5846.

60. Li Z; Gelbaum C; Fisk JS; Holden B; Jaganathan A; Whiteker GT; Pollet P; Liotta CL Aqueous Suzuki coupling reactions of basic nitrogen-containing substrates in the absence of added base and ligand: Observation of high yields under acidic conditions. J. Org. Chem 2016, 81, 8520–8529. [PubMed: 27559749]

61. Zhou L; Yang L; Tilton S; Wang J Development of a high throughput equilibrium solubility assay using miniaturized shake-flask method in early drug discovery. J. Pharm. Sci 2007, 96, 3052–3071. [PubMed: 17722003]
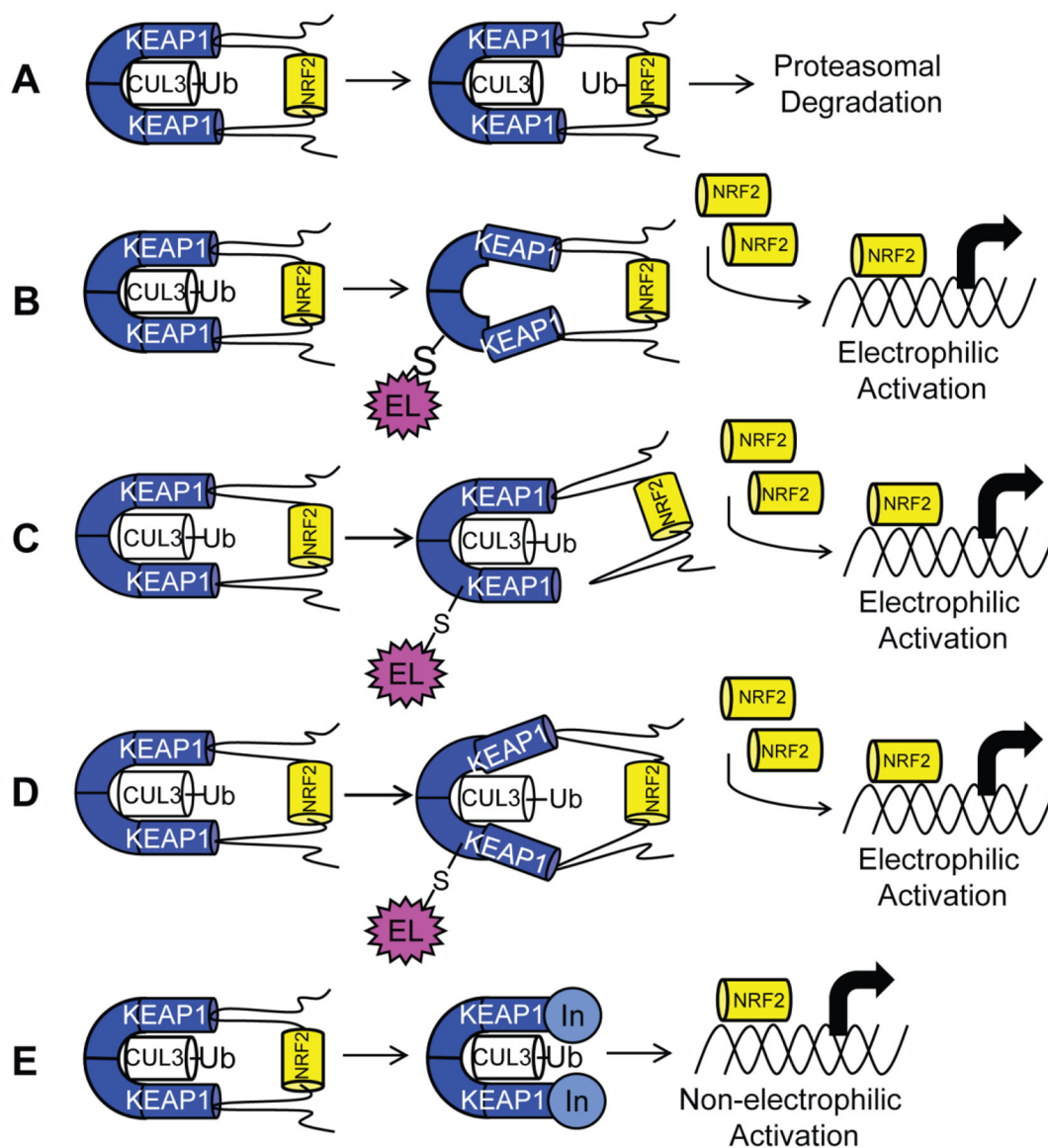
Figure 1:

(A) Transcription factor NRF2, when bound to substrate adaptor KEAP1, is ubiquitinated by E3 ligase CUL3, leading to proteosomal degradation. Two mechanisms explain activation of NRF2 by electrophiles. **(B)** In the CUL3 dissociation mechanism, cysteine modification by an electrophile causes dissociation of CUL3, leading to accumulation of NRF2. **(C)** In the hinge-and-latch mechanism, cysteine modification causes non-optimal placement of NRF2 for degradation. **(D)** In the conformational cycling model, cysteine modification locks KEAP1 and NRF2 in a conformation not ideal for ubiquitination, preventing KEAP1 from binding nascent NRF2, leading to accumulation of NRF2 **(E)** The non-electrophilic mechanism aims to create a non-covalent inhibitor of the protein-protein interaction between KEAP1 and NRF2 to activate NRF2.
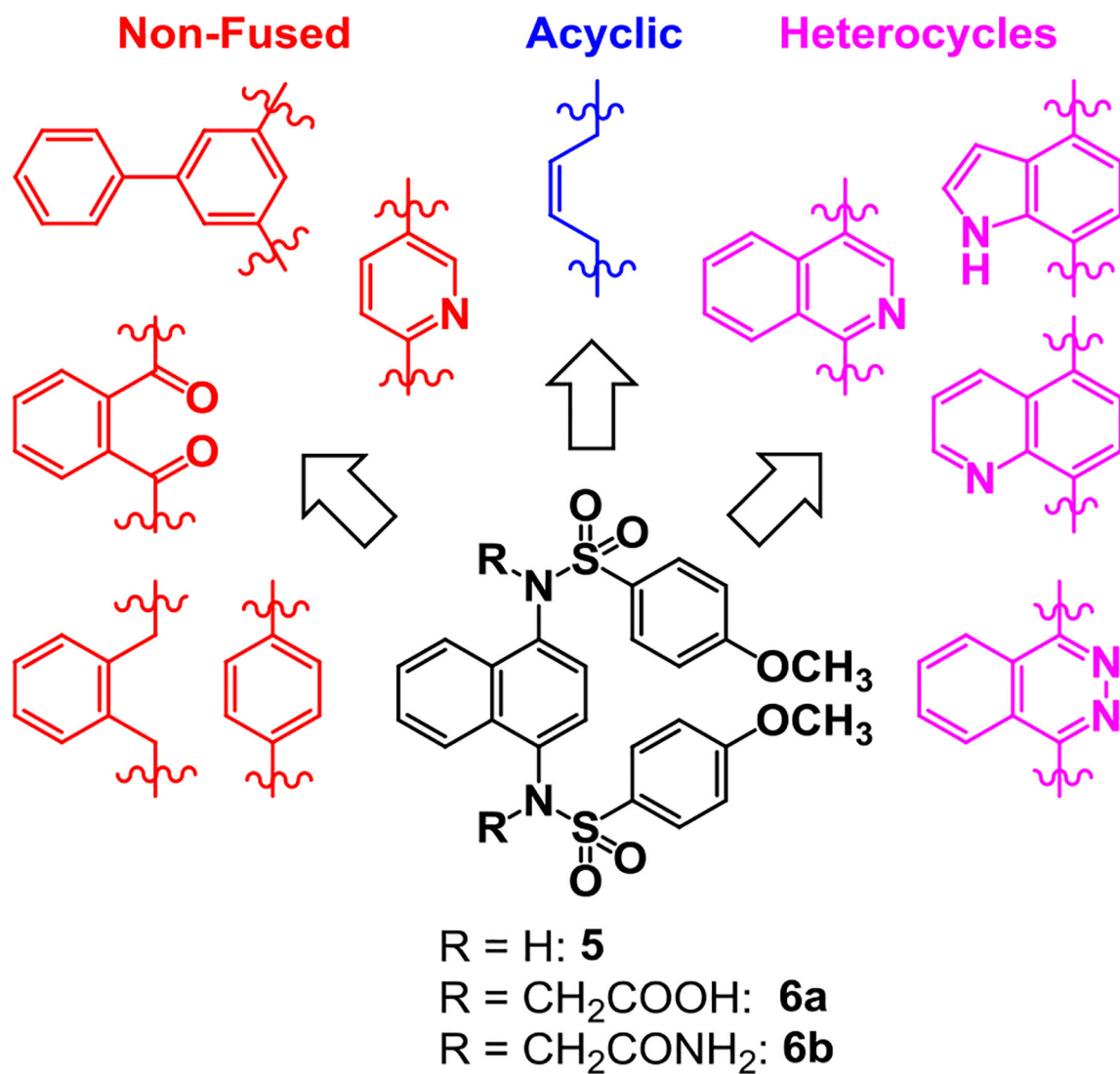
Figure 2:
Non-fused (red), acyclic (blue) and heterocyclic (magenta) analogs were designed to replace the naphthalene core of non-covalent NRF2 activators.
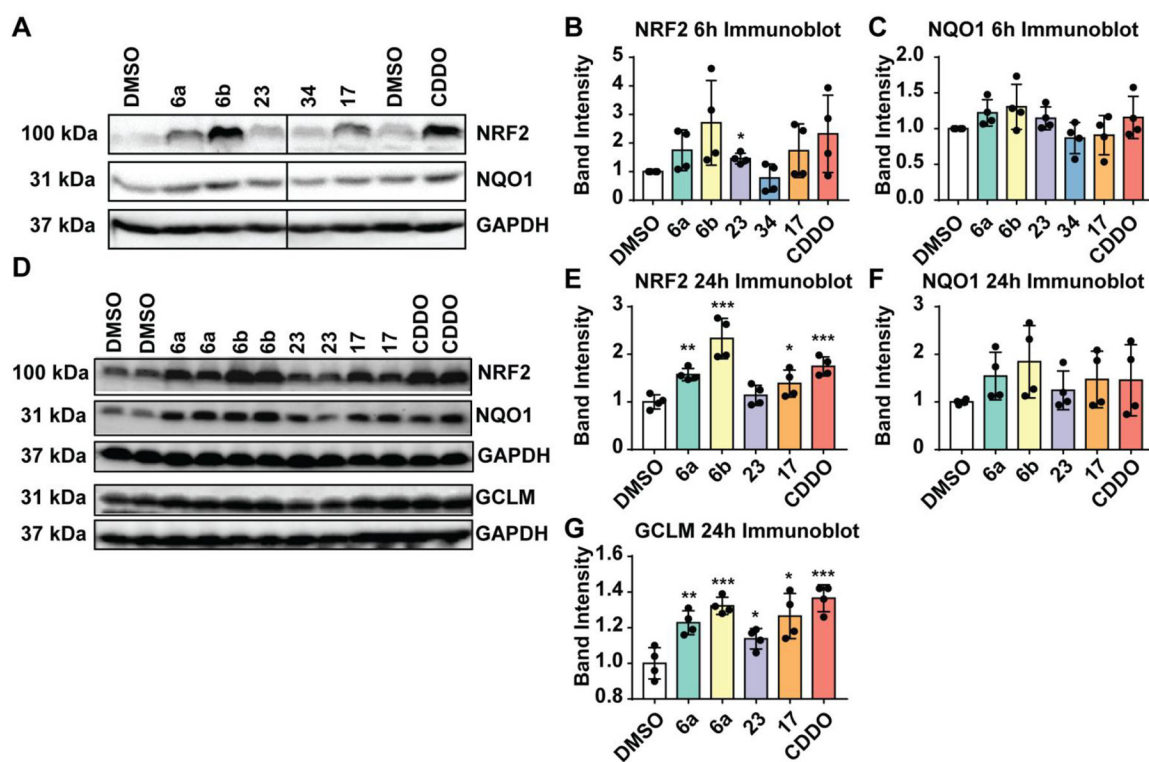
Figure 3:
HaCaT cells were treated with 10 μM compound (**6a, 6b, 17, 23**; positive control **CDDO-Im**) or vehicle (DMSO) for 6 h (**A**) or 24 h (**D**) as shown in the immunoblots. Cell lysates were prepared, equal amount of protein was probed with antibodies specific for NRF2, NQO1 or GCLM. GAPDH was used as a reference. Quantification of band intensities of NRF2 (**B, E**), NQO1 (**C, F**) and GCLM levels (**G**) are shown. DMSO-treated sample values were used as one arbitrary unit.*:$p<0.05$; **:$p<0.01$; ***:$p<0.001$; if no * is indicated, $p>0.05$.

Figure 4:

The effects of non-electrophilic activators **17** (orange) and **23** (purple) and positive control **CDDO-Im** on the nuclear accumulation of NRF2 in HaCaT Cells. (**A**) HaCaT cells were treated with DMSO (vehicle) or indicated compound (10 μM) for 6 hours and 24 hours, Nuclear (N) and cytosolic (C) fractions were prepared, equal amount of protein was immunoblotted using antibodies specific for NRF2. β-actin / Lamin A/C was used as loading control. (**B**) Quantification of Nrf2 band intensity using β-actin as reference. DMSO-treated sample value was used as one arbitrary unit. Error bars represent the standard error from four independent experiments. *:$p<0.05$; **:$p<0.01$; ***:$p<0.001$; if no * is indicated, $p>0.05$.

Figure 5:

The effects of non-electrophilic activators **17** (orange) and **23** (purple) on NRF2 target gene expression in HaCaT Cells. (A) HaCaT cells were treated with DMSO (vehicle) or indicated compound (10 μM) for 6 hours and 24 hours. cDNA were prepared from mRNA and analyzed for the target gene expression (**A**: *HMOX1*; **B**: *NQO1*; **C**: *GCLC*; **D**: *GCLM*; **E**: *SOD*) using qPCR with specific primers. Relative fold change was calculated with β-actin as reference. DMSO-treated sample value was used as one unit. Error bars represent the standard error from 3–4 independent samples. *:$p<0.05$; **:$p<0.01$; ***:$p<0.001$; if no * is indicated, $p>0.05$.
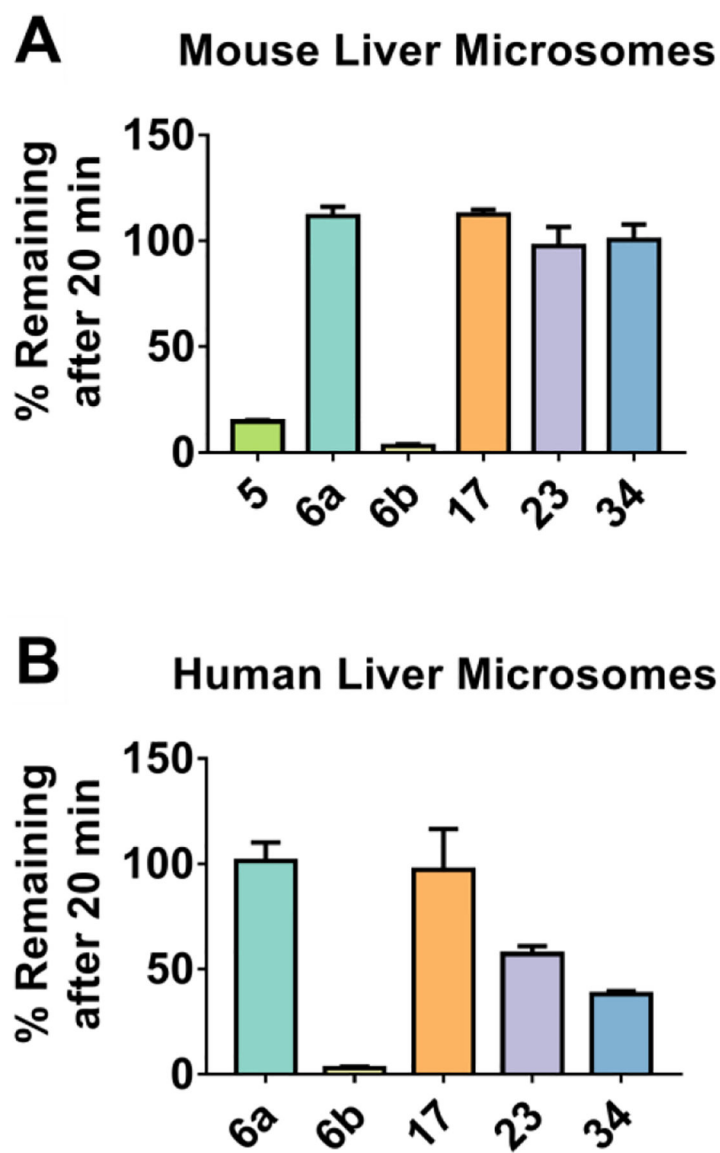
Figure 6: Stability to Liver Microsomes.
Compounds were incubated with mouse liver microsomes (**A**) and human liver microsomes (**B**) for 20 min. Percentage of compound remaining after incubation was determined by LC-MS.
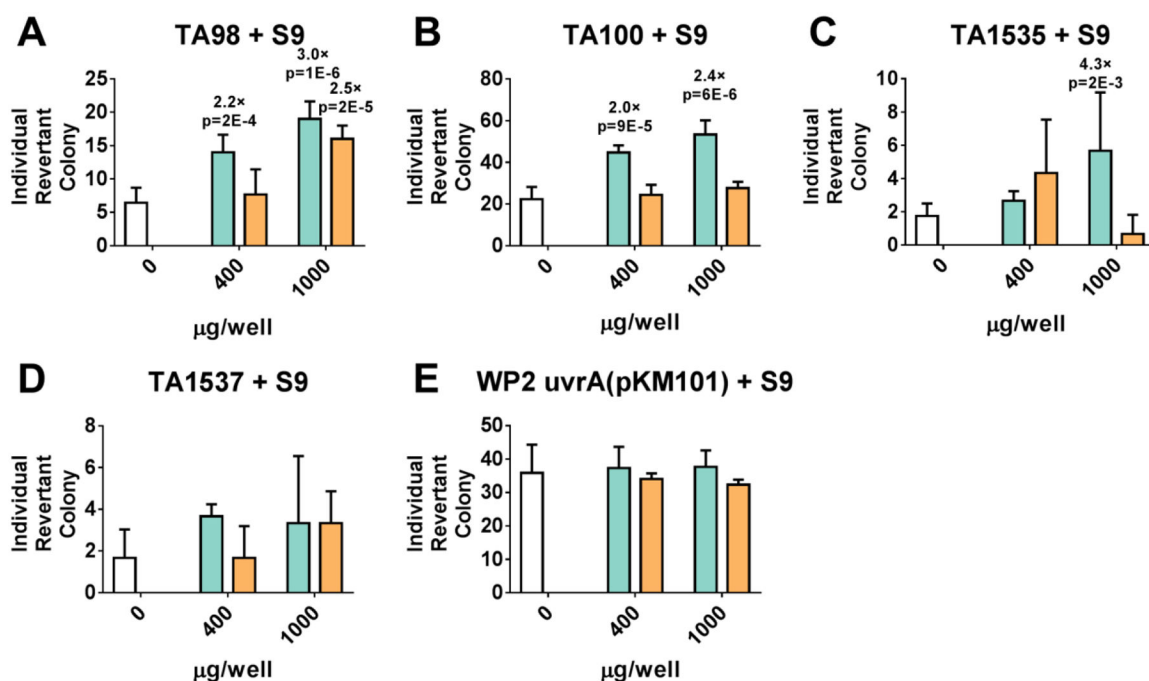
Figure 7: Mini-Ames Assay Results.
Compounds **6a** (turquoise) and **17** (orange) and vehicle control DMSO (white) were tested for their ability to induce reverse mutations at the histidine locus of strains TA98 (**A**), TA100 (**B**), TA1535 (**C**), and TA1537 (**D**) of *Salmonella typhimurium* and strain WP2 uvrA(pKM101) (**E**) of *Escherichia coli* in the presence of exogenous rat liver S9 fractions. Individual revertant colonies were counted and graphed as a function of compound concentration (400 and 1000 μg/well). Fold-change for those conditions that were >2.0× greater than DMSO vehicle control are shown above each bar, along with *p*-values determined from a two-tailed t-test.
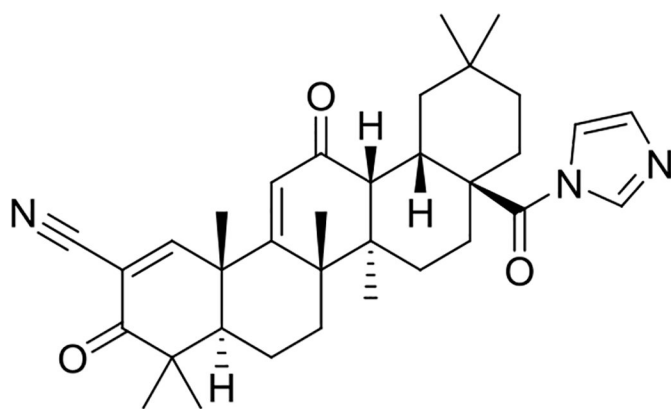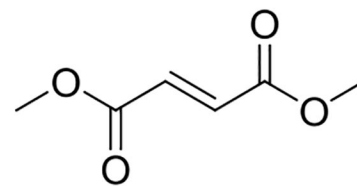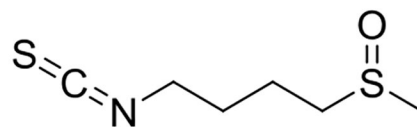
Chart 1:
Electrophilic activators of NRF2
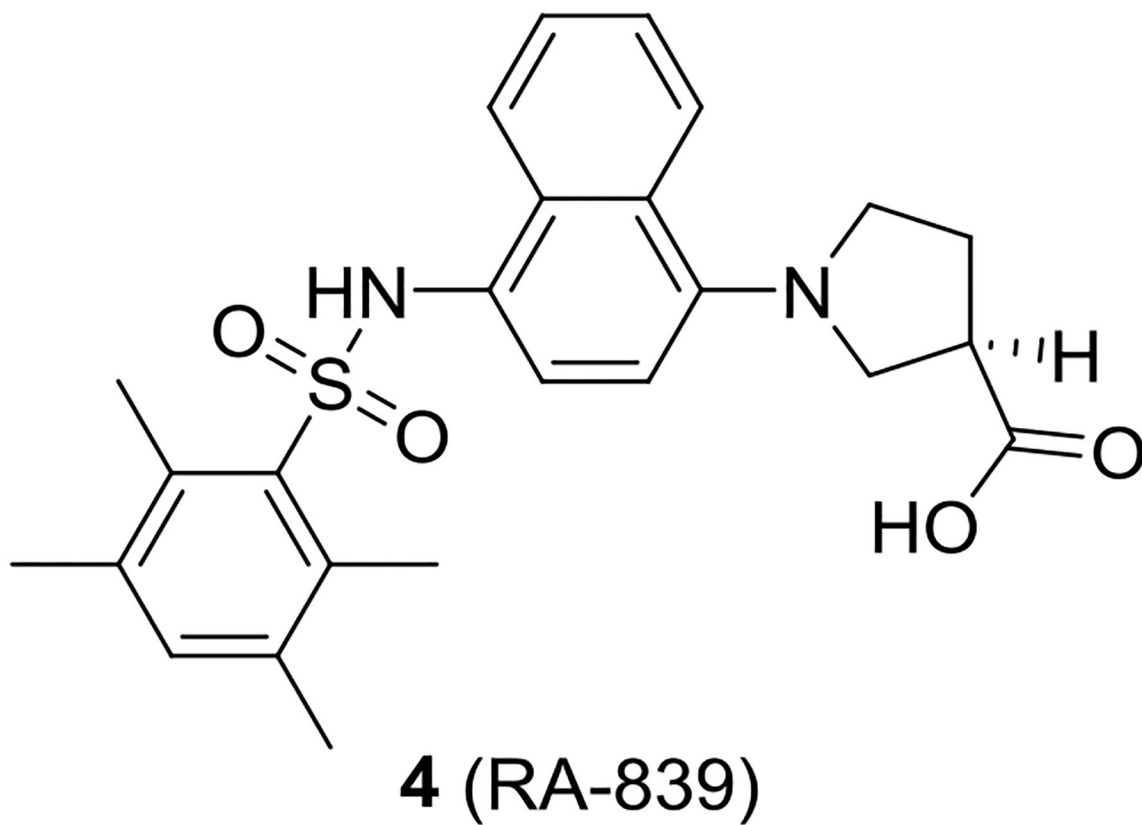
4 (RA-839)

Chart 2:
Naphthalene **4** (RA-839) is active *in vivo* only if Phase 1 metabolism is inhibited.
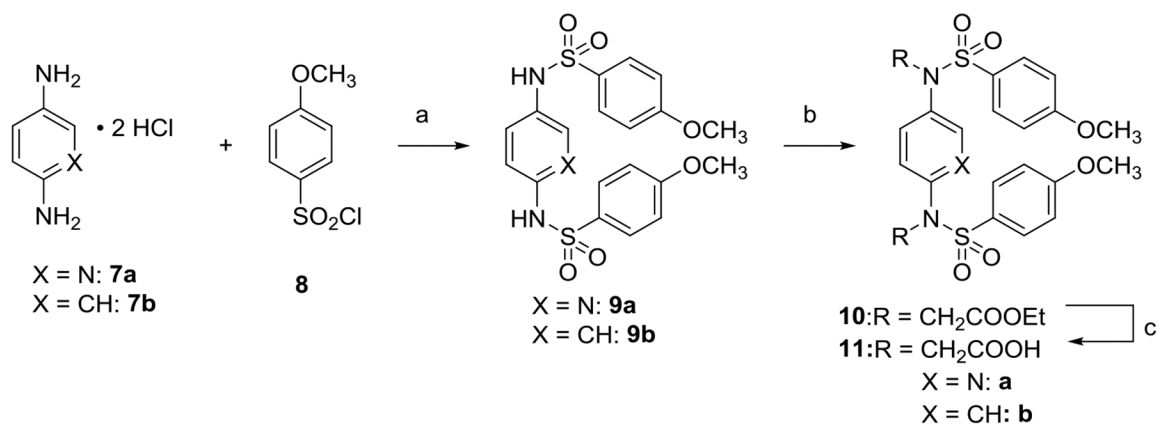
Scheme 1. Synthesis of compounds 11a and 11b[a]

[a]Reagents: (a) pyridine, rt, 18–76% yield; (b) RBr, K_2CO_3, DMF, rt, 80% yield; (c) NaOH, MeOH, reflux. 67–80% yield; rt: room temperature
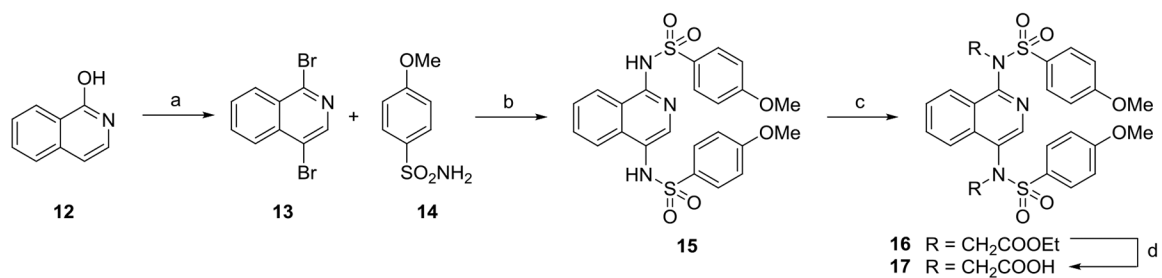
Scheme 2. Synthesis of 1,4-isoquinolines 15 and 17[a]

[a]Reagents: (a) PBr_5, 140 °C, 89% yield; (b) CuI, *N,N'*-dimethylethylenediamine, K_2CO_3, MeCN, 70 °C, 60% yield; (c) RBr, K_2CO_3, DMF, rt, 77% yield; (d) NaOH, MeOH, reflux, 36% yield. rt: room temperature
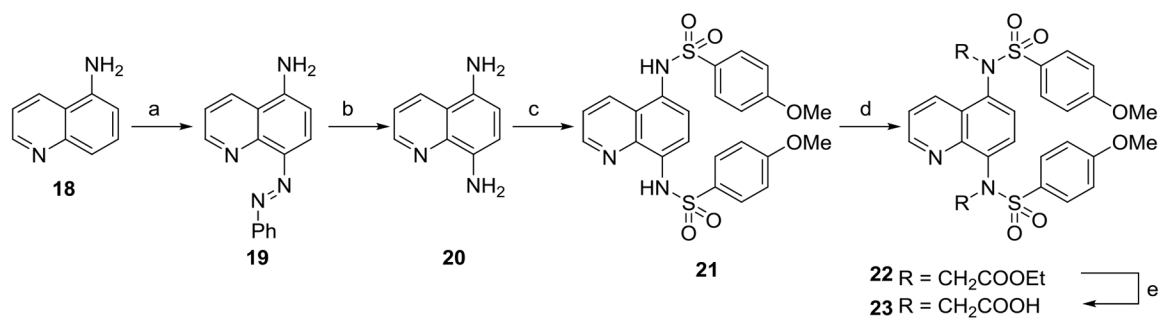
Scheme 3. Synthesis of quinolines 21 and 23[a]

[a]Reagents: (a) aniline, NaNO₂, HCl, AcOH, NaOAc, H₂O, 30% yield; (b) SnCl₂, HCl, reflux, 50% yield; (c) *p*-methoxybenzenesulfonyl chloride, pyridine, rt, 77% yield; (d) RBr, K₂CO₃, DMF, rt; (e) NaOH, MeOH, reflux, 67% yield over 2 steps. rt: room temperature
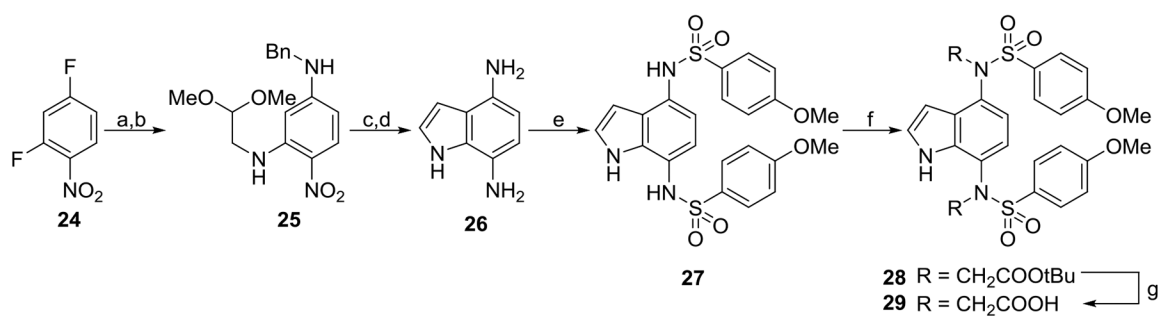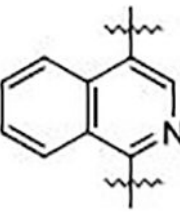
Scheme 4. Synthesis of indoles 27 and 29[a]

[a]Reagents: (a) aminoacetaldehyde dimethyl acetal, i-Pr$_2$NEt, MeOH, reflux, 86% yield; (b) benzylamine, 1,4-dioxane, reflux, 93% yield; (c) F$_3$CCO$_2$H, CH$_2$Cl$_2$, rt, 85% yield; (d) Pd/C, EtOH/HCl, H$_2$, 35 psi, 100% yield; (e) p-methoxybenzenesulfonyl chloride, pyridine, rt, 60% yield; (f) RBr, K$_2$CO$_3$, DMF, rt, 82% yield; (g) TFA, CH$_2$Cl$_2$, rt, 20% yield. rt: room temperature
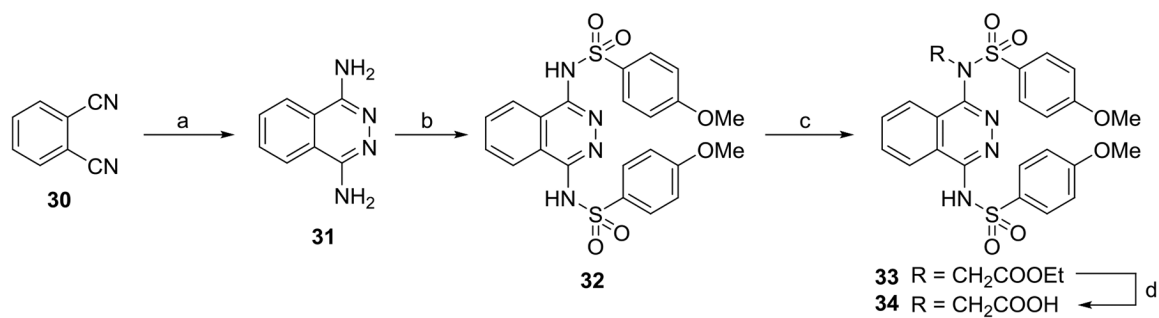
Scheme 5. Synthesis of phthalazines 32 and 34[a]

[a]Reagents: (a) NH$_2$NH$_2$, MeOH, rt, reflux, 65% yield; (b) pyridine, 1,4-dioxane, reflux, 31% yield; (c) ethyl bromoacetate, Li^{t}BuO, DMF, rt, 100% yield; (d) NaOH, MeOH/H$_2$O, 54% yield. rt: room temperature
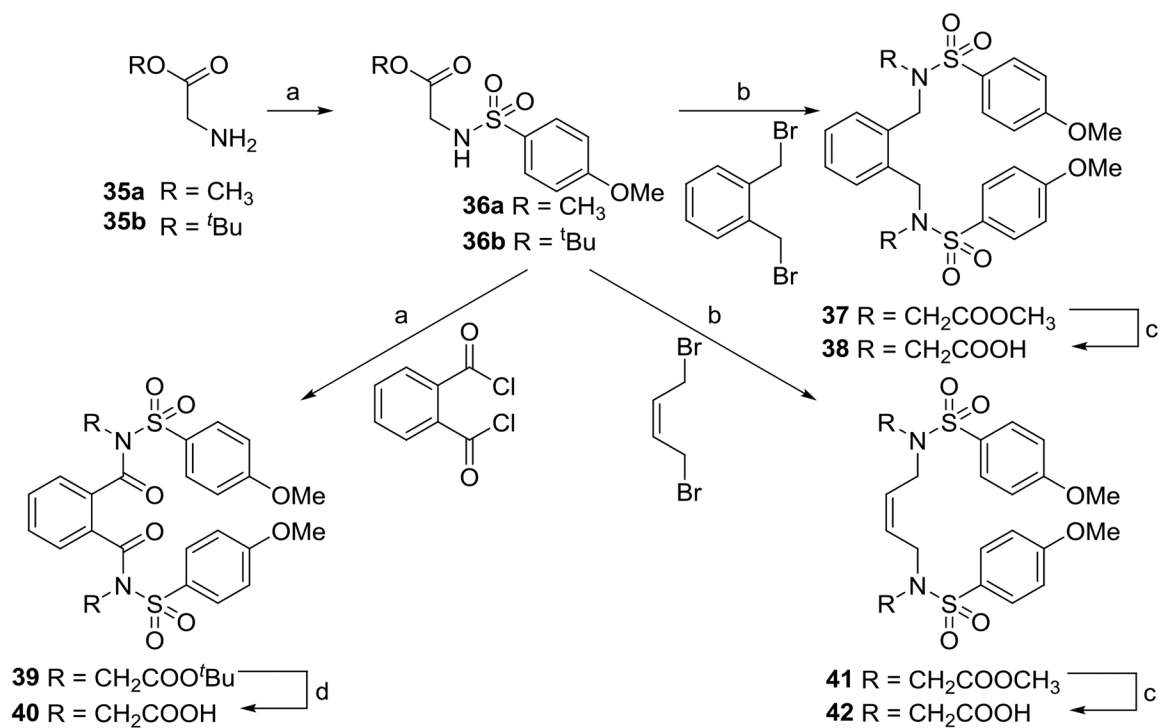
Scheme 6. Synthesis of compounds 38, 40, and 42[a]

[a]Reagents: (a) pyridine, rt 55–58% yield; (b) RBr, K_2CO_3, DMF, rt, 70–80% yield; (c) NaOH, MeOH, reflux, 70–74% yield; (d) F_3CCO_2H, CH_2Cl_2, rt, 55% yield. rt: room temperature
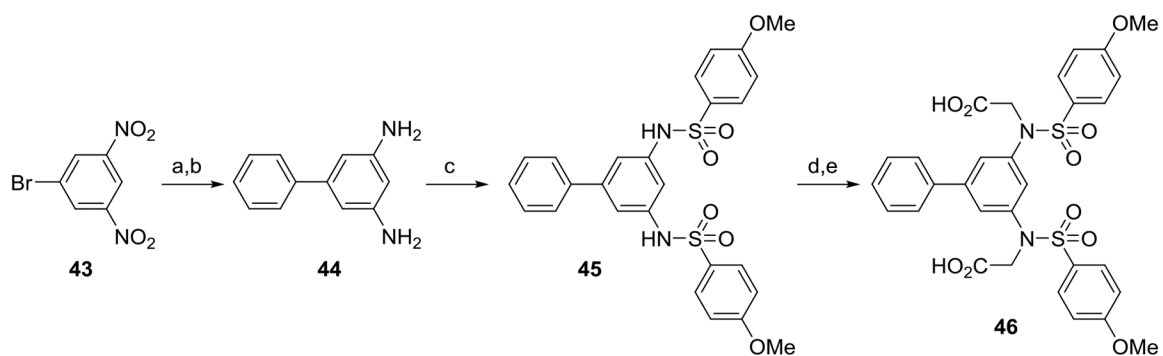
Scheme 7. Synthesis of biphenyl 46

[a]Reagents: (a) phenylboronic acid, Pd(OAc)$_2$, K$_3$PO$_4$, H$_2$O, reflux, quant. yield; (b) SnCl$_2$, MeOH, reflux, 99% yield; (c) *p*-methoxybenzenesulfonyl chloride, pyridine, THF, reflux; (d) ethyl bromoacetate, K$_2$CO$_3$, DMF; (e) NaOH, MeOH, reflux, 51% yield over 3 steps. rt: room temperature
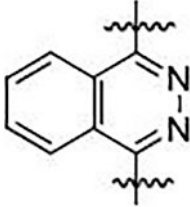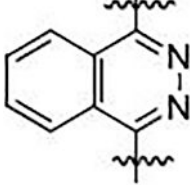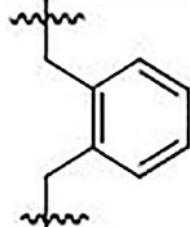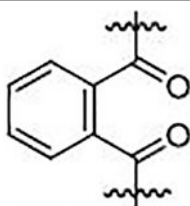
Table 1:
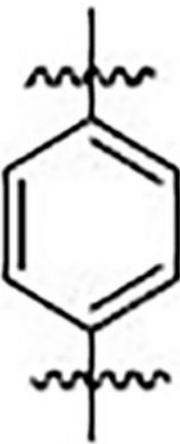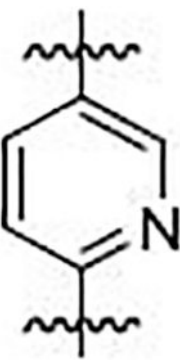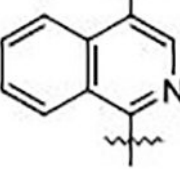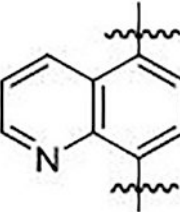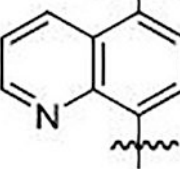
IC$_{50}$ and K$_d$ values.
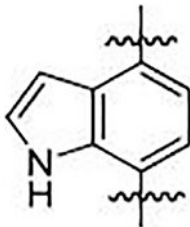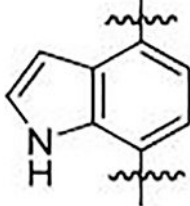
IC$_{50}$ values, shown in nM units with 95% confidence intervals, were determined by fluorescence anisotropy. K$_d$ values, shown in nM units ± standard deviation, were determined by surface plasmon resonance. [a]Fluorescent interference from **15** impeded accurate determination of IC$_{50}$. [b] IC$_{50}$ and K$_d$ values reported in Jain et al.[1]. ND = Not determined
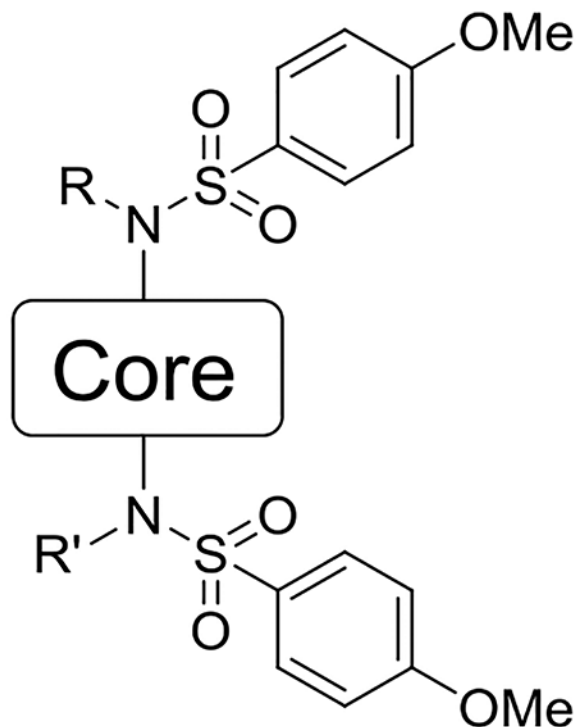
Compound	Core	R	R'	IC$_{50}$ (nM) (95% CI)	K$_d$ (nM)
5		–H	–H	940 [b] (850 – 1300)	1700 ± 120 [b]
6a		–CH$_2$COOH	–CH$_2$COOH	25 [b] (19–31)	20 ± 3 [b]
6b		–CH$_2$CONH$_2$	–CH$_2$CONH$_2$	63 [b] (52 – 85)	44 ± 8 [b]

Compound	Core	R	R'	IC_{50} (nM) (95% CI)	K_d (nM)
9b		–H	–H	>25000	ND
11b		–CH$_2$COOH	–CH$_2$COOH	980 (600–1600)	ND
11a		–CH$_2$COOH	–CH$_2$COOH	>25000	ND
15		–H	–H	ND[a]	ND
17		–CH$_2$COOH	–CH$_2$COOH	60 (30–110)	102 ± 16
21		–H	–H	>25000	ND
23		–CH$_2$COOH	–CH$_2$COOH	101 (80–130)	103 ± 2

Compound	Core	R	R'	IC$_{50}$ (nM) (95% CI)	K_d (nM)
27		–H	–H	>25000	ND
29		–CH$_2$COOH	–CH$_2$COOH	1300 (390–5400)	ND
32		–H	–H	>25000	ND
34		–CH$_2$COOH	–H	1100 (435–2500)	> 10 μM
38		–CH$_2$COOH	–CH$_2$COOH	>25000	ND
40		–CH$_2$COOH	–CH$_2$COOH	>25000	ND
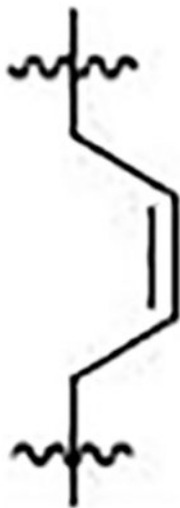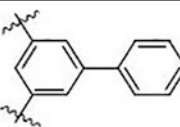
Compound	Core	R	R'	IC$_{50}$ (nM) (95% CI)	K_d (nM)
42		−CH$_2$COOH	−CH$_2$COOH	>25000	ND
46		−CH$_2$COOH	−CH$_2$COOH	>25000	ND

Table 2:

Aqueous solubility, shown in μM units ± standard deviation.

Compound	Aqueous Solubility (μM)
5	5.4 ± 0.9
6a	440 ± 3
6b	22 ± 9
9b	1.2 ± 0.2
11b	1.2 ± 0.2
11a	190 ± 0.8
15	3.8 ± 0.1
17	380 ± 3
21	6.1 ± 0.1
23	390 ± 4
27	0.86 ± 0.3
29	N.D.[b]
32	370 ± 7
34	380 ± 7
38	1.3 ± 0.3
40	490 ± 90
42	420 ± 12
46	270 ± 3

Table 3.

MRM transitions (precursor ion Q1, product ion Q3) and compound related parameters (Q1 Pre Bias, CE, Q3 Pre Bias)

Compound Name	Q1	Q3	Q1 Pre Bias	CE	Q3 Pre Bias
34	559.0	107.0	−26	−53	−16
6a	613.1	170.9	30	40	18
17	616.1	428.1	−30	−20	−19
23	616.0	274.0	−30	−28	−27
6b	581.1	426.1	−20	−13	−28